DOI: https://doi.org/10.3986/ac.v52i1.10687

ASSESSMENT OF THE HYDROGEOCHEMICAL AND ISOTOPIC CHARACTERIZATION AND HYDRAULIC BEHAVIOR OF THE IZEH COMPLEX KARSTIC AREA, KHUZESTAN PROVINCE, SOUTHWEST IRAN

HIDROGEOKEMIČNA IN IZOTOPSKA KARAKTERIZACIJA TER OCENA HIDRAVLIČNEGA DELOVANJA KOMPLEKSNEGA KRAŠKEGA OBMOČJA IZEH, PROVINCA KHUZESTAN, JUGOZAHODNI IRAN

Nasrollah KALANTARI[1]*, Zahra SAJADI[2], Abbas CHARCHI[3] & Seyyed Sajedin MOUSAVI[4]

Abstract UDC 550.42:532.5:556(55)

Nasrollah Kalantari, Zahra Sajadi, Abbas Charchi & Sayyed Sajedin Mousavi: Assessment of the hydrogeochemical and isotopic characterization and hydraulic behavior of the Izeh complex karstic area, Khuzestan province, southwest Iran

Proper water resources management requires recognizing and evaluating the factors that affect the quantity and quality of water resources. The Ilam-Sarvak (Upper Cretaceous) and Asmari (Oligocene to Miocene) limestone- dolomite formations in the Zagros structural belt have formed a promising karst groundwater horizon. In the present study, the hydraulic relationship between the karst structures of the Izeh territory in the northeast of Khuzestan province was investigated using hydrogeochemical and isotopic information of springs and wells. The results enabled to understand various components influencing the recharge of water resources. In this study, samples were collected from the karst springs and wells of Mongasht, Shavish-Tanosh and Kamarderaz anticlines and Naal-e-Asbi (Horseshoe) syncline and meteoric water to understand the hydrochemical and isotopic characterization, and hydrogeological and hydraulic behavior of the Izeh karst system. The meteoric and groundwater samples were analyzed to determine major and minor ion concentrations and $\delta^{18}O$ and $\delta^{2}H$ isotope ratios. Isotopic content ranged from -31.6 to -2.9‰ and from -6.32 to -1.87‰ for $\delta^{2}H$ and $\delta^{18}O$, respectively, and d-excess values were high and positive. The study of the isotopic content of water

Izvleček UDK 550.42:532.5:556(55)

Nasrollah Kalantari, Zahra Sajadi, Abbas Charchi & Sayyed Sajedin Mousavi: Hidrogeokemična in izotopska karakterizacija ter ocena hidravličnega delovanja kompleksnega kraškega območja Izeh, provinca Khuzestan, jugozahodni Iran

Ustrezno gospodarjenje z vodnimi viri temelji na prepoznavanju in vrednotenju dejavnikov, ki vplivajo na količino in kakovost vodnih virov. Apnenčasto-dolomitni formaciji Ilam-Sarvak (zgornja kreda) in Asmari (oligocen do miocen) v strukturnem pasu Zagros sta oblikovali obetaven kraški vodonosnik. V tej študiji je bil hidravlični odnos med kraškimi strukturami ozemlja Izeh, ki je na severovzhodu province Khuzestan, ocenjen z uporabo hidrogeokemičnih in izotopskih analiz vode v izvirih in vodnjakih. Rezultati so omogočili razumevanje komponent, ki vplivajo na napajanje vodnih virov. Zbrani so bili vzorci iz kraških izvirov in vodnjakov antiklinal Mongašt, Šaviš-Tanoš, Kamarderaz, sinklinale Naal-e-Asbi (podkev) in meteorne vode, da bi razumeli hidrokemično in izotopsko karakterizacijo ter hidrogeološko in hidravlično delovanje kraškega sistema Izeh. Za določitev koncentracij glavnih in drugotnih ionov ter razmerja izotopov $\delta^{18}O$ in $\delta^{2}H$ so bili analizirani vzorci meteorne in podzemne vode. Vsebnosti izotopov so bile v razponu od −31,6 do −2,9 ‰ za $\delta^{2}H$ in od −6,32 do −1,87 ‰ za $\delta^{18}O$, vrednosti devterijevega presežka pa so bile visoke in pozitivne. Analize vsebnosti izotopov v vzorcih vode iz izvirov in vodnjakov v regiji kažejo na tri skupine vodnih virov. Prva skupina, ki je povezana z izviri

[1] Faculty of Earth Sciences, Shahid Chamran University of Ahvaz, Iran, e-mail: nkalantari@hotmail.com, n.kalantari@scu.ac.ir
[2] Faculty of Earth Sciences, Shahid Chamran University of Ahvaz, Iran, e-mail: sajadi_z@yahoo.com
[3] Faculty of Earth Sciences, Shahid Chamran University of Ahvaz, Iran, e-mail: charchi38@scu.ac.ir
[4] Faculty of Earth Sciences, Shahid Chamran University of Ahvaz, Iran, e-mail: s.mousavi@scu.ac.ir
* Corresponding author

Prejeto/Received: 24.2.2022

samples of springs and wells in the region shows three groups of water sources. The first group, related to the Mongasht anticline springs, has lower isotopic values, indicating that it is recharged by rainfall at high altitudes and snow melting. The isotopic value of the second group is richer than that of the first group, indicating rainfall recharge as well as groundwater mixing (examples of Naal-e-Asbi syncline and Shavish-Tanosh anticline). The highest value in the third group (samples of Kamarderaz anticline) is attributed to evaporation and longer distance from the recharge site to the discharge point, as well as to the diffusion system. The trend of decrease in Sr+2 and increase in Ba+2 in the samples of dolomitic limestone formations (Shavish Tanosh and Mongasht anticlines) compared to the water samples of Kamarderaz anticline and Naal-e-Asbi syncline indicates the possibility that karst aquifers of the region are recharged from the Mongasht anticline and that there is a hydraulic relationship between these structures. D-excess and $\delta^{18}O$ show a linear trend, illustrating the effect of altitude difference on isotopic content and recharge sources. The major and minor changes in the concentration of ions, the isotopic content of groundwater and the relationship between TDS and $\delta^{18}O$ and d-excess and $\delta^{18}O$ indicate the mixing and recharging of karst aquifers (Shavish-Tanosh, Kamarderaz and Naal-e-Asbi aquifers) from the Mongasht karst aquifer and their hydraulic connection.
Keywords: Izeh, chemical, isotopes, karst, hydraulic connection.

antiklinale Mongašt, ima nižje izotopske vrednosti, kar kaže, da se napaja s padavinami na višjih nadmorskih višinah in s taljenjem snega. Izotopska vrednost druge skupine je bogatejša od prve skupine, kar kaže na napajanje s padavinami in na mešanje podzemnih vod (primera sinklinale Naal-e-Asbi in antiklinale Šaviš-Tanoš). Najvišja vrednost v tretji skupini (vzorci antiklinale Kamarderaz) je posledica delno izhlapevanja in daljše razdalje med mestoma napajanja in iztekanja ter delno difuzijskega sistema. Trend padanja Sr^{2+} in naraščanja Ba^{2+} v vzorcih v formacijah dolomitnih apnencev (antiklinali Šaviš-Tanoš in Mongašt) v primerjavi z vzorci vode antiklinale Kamarderaz in sinklinale Naal-e-Asbi kaže na možnost, da se kraški vodonosniki napajajo iz območja antiklinale Mongašt, in na hidravlični odnos med temi strukturami. Devterijev presežek in $\delta^{18}O$ kažeta linearni trend, ki ponazarja učinek višinske razlike na vsebnost izotopov in vire napajanja. Večje in manjše spremembe v koncentraciji ionov, vsebnosti izotopov v podzemni vodi in razmerju med TDS in $\delta^{18}O$ ter devterijevim presežkom in $\delta^{18}O$ kažejo na mešanje in napajanje kraških vodonosnikov (vodonosniki Šaviš-Tanoš, Kamarderaz in Naal-e-Asbi) s kraškega vodonosnika Mongašt in na njihovo hidravlično povezanost.
Ključne besede: Izeh, kemijski, izotopi, kras, hidravlična povezava.

1. INTRODUCTION

For groundwater supply to be managed sustainably in water scarce regions, understanding the sources of recharge and flow pattern of groundwater in these regions is imperative. The hydrochemical and stable isotope techniques have been commonly employed to identify groundwater recharge mechanisms and flow paths (Scanlon et al., 2002; Gates et al., 2008; Slabe & Liu, 2009; Bourke et al., 2015; Connor et al., 2017; Chen et al., 2018; Morsy et al., 2018; Mokadem et al., 2021). During the last three decades, chemical constituents and the isotopic composition of water have been widely used to characterize the groundwater recharge sources, recharge rate and flow pattern and therefore address associated resource problems (Bajjali, 2006; Edmunds et al., 2006; Ma et al., 2013).

Karst regions have a specific hydrogeological character (Milanovic, 1981; Ford & Williams, 1989, 2007) because the constituent rocks, like limestone and dolomite, are highly susceptible to chemical dissolution (Milanovic, 1981; Goldscheider & Andreo, 2007). In the karstic regions, the study of chemistry is essential (White, 2015) because hydrochemical properties reflect the mechanism of groundwater flow in karstic rocks. Karst aquifers have heterogeneous characteristics owing to the three media-based systems through which groundwater flows, namely pores, fractures, and cavities (Goldscheider & Andreo, 2007).

The chemical constituents of groundwater illustrate a key role in evaluating the quality of water. In unpolluted groundwater systems, major and minor ions composition is controlled by several factors like geology, water-rock interaction and recharge water (Krienen et al., 2017; Pracny et al., 2017; Jebreen et al., 2018; Ventura-Houle et al., 2021). As it is known, water contains dissolved ions that affect the physical and chemical properties of water. Therefore, scientists continue to investigate the physical and chemical properties of groundwater (Wang et al., 2018; Rehman et al., 2019; Farid et al., 2020; Haldar et al., 2020; Yasin & Kargın, 2021). Studies of karst hydrogeological systems using hydrochemical and stable isotope analyses (^{18}O and ^{2}H) have been conducted by Ashjari and Raeisi (2006), Dimitriou and Tsintza (2015), Alemayehu et al. (2020), Setiawan et al. (2020) while the more specific study employing multivariate hydrochemical analysis has also been conducted by e.g., Valdes et al. (2007); Narany et al. (2014); Chihi et al. (2015) and Yuan et al. (2017). These studies generally explain hydrochemical processes such as dissolution and precipitation of carbonate minerals, and identification of karstic hydrogeological systems, including; the process of karst groundwater recharge, flow pattern, and discharge.

The isotopes ^{18}O and ^{2}H are conservative (Tillman et

al., 2014; Murillo et al., 2015; Sun et al., 2016; Heydarizad et al., 2021; Mokadem et al., 2021; Tian et al., 2021; Vreca & Kern, 2021) that is, not seriously affected by water–rock interaction processes at low temperatures (Marfia et al., 2004). These isotopes have been used in studies of groundwater recharge and flow direction (Marfia et al., 2004; Rodgers et al., 2005; Blasch & Bryson, 2007; Ryu et al., 2007; Singh et al., 2013(, the heterogeneity of aquifer hydraulic properties (Marfia et al., 2004; Doveri et al., 2013), residence time of groundwater (Rademacher et al., 2003; Mahlknecht et al., 2006), and also the mixing of groundwater from different sources (Coplen, 1993). Several studies have suggested the application of hydrochemical and isotopic tracers to elucidate sources of dissolved ions and hydrogeochemical processes that controls the chemical variability in the multilayered aquifer system (Wang et al., 2018; Liu et al., 2019). Hydrochemistry and stable isotopes are employed for spring discharge studies (Doctor et al., 2006; Hatipoglu-Bagci & Sazan, 2014). Likewise, delineation of the recharge area and distinguishing sources of recharge to the karstic springs have been accomplished by applying hydrochemistry and stable isotopes (Blasch & Bryson, 2007; Bhat & Jeelani, 2015).

The Izeh plain contains over 60 deep and semi-deep alluvial wells which are utilized for irrigation, but the yield and quality of groundwater are poor due to fine grain sediments. In the karstic terrain of the Izeh area, 21 deep karstic wells are merely exploited for drinking purpose and on average the annual withdrawal is about 20 Mm^3. It is to be noted that groundwater extraction from these karstic aquifers is very important and crucial in terms of drinking water supply for Izeh City and surrounding villages. Though, a large number of small karstic springs with low discharge (between 1 to 5 l/s) are distributed in different parts of the area, but the outstanding spring is emerging from the western limb of the Monghasht anticline is known as Mal -Agha. On average the annual spring discharge is 1.5 m^3 /s which is a significant water supply for another sub-catchment relatively away from the Izeh area.

The geological formations of the Izeh complex karstic terrain are mainly calcareous, but with respect to lithology, morphology and structure are more or less different (existence of anticlines and synclines with different lithology). Integration of the abundant information gathered from different sources is crucial for developing knowledge about the karstic aquifers and their interconnection. As hydrochemistry and stable isotopes provide key information to characterize hydraulic connectivity so, in this work, hydrochemistry including major and minor ions and stable isotopes ($\delta^{18}O$ and $\delta^{2}H$) of the main karst springs and exploitation wells in the Izeh area were taken into account- to designate the hydrochemical and isotopic behavior of the Izeh karstic terrain and to determine hydraulic interconnection among the karstic aquifers.

1.1. STUDY AREA

The study area (Figure 1) occupies 910 km^2 and is located between longitude 49° 56′ 30" to 50° 26′ 33" east and latitude 31° 26′ 03" to 31° 53′ 00" north at a distance of almost 183 km in the north east of the Ahvaz City (capital of Khuzestan province). The area experiences a semi-arid climatic condition and, based on 30 years data (1990-2020), the mean annual temperature is 20.7 °C, and the lowest (5.9 °C) and the highest temperatures (33 °C) were recorded in the February and July respectively. The average annual real evapotranspiration from the free surface of water is 1,632 mm. The average annual rainfall of the area is 760 mm and commonly occurs as thunderstorms in the late autumn to early spring. In spite of relatively high rainfall, the Izeh area suffers from shortage of water resources and relies on only groundwater for different consumptions. The great Karun River with 200 m^3/s average annual discharge flows in the northern part of the study area, but water supply from the river in the study area is crucial due to the mountainous nature of the command area. On the other hand, the Izeh alluvial plain is mainly composed of the fine clay-silty sediments and essentially poor for water infiltration, percolation and accumulation forming a promising aquifer.

1.2. GEOLOGICAL SETTING

From the geological point of view, the study area is situated on the southern flank of the folded Zagros domain in the Zagros Mountain Range (Stocklin, 1974; Alavi, 1996) that evolved by different orogeny during the Cimmerian and Alpine orogeny (Alavi, 1996; Zanchi et al., 2009). Such geological events resulted in an extremely complex geology and asymmetric structures (Stocklin, 1974); however, the Cenozoic compressional events masked almost all of the earlier structural events data.

The main exposed geological formations in the area with respect to age include Daryan-Fahlian limestone (Lower Cretaceous), Ilam-Sarvak limestone-dolomite (Upper Cretaceous), Asmari limestone (Oligocene to Miocene) and the Shaly-Marly Pabdeh-Gorpi formation (Upper Cretaceous to Eocene). The majority of the geological structure (folds and fault), including Mongasht, Shavish-Tanosh, Kamarderaz anticlines, and the Naal-e-Asbi are trending NW–SE.

The asymmetrical single limb Kamarderaz anticline trending NW-SE, extending parallel to the Shavish-Tanosh anticline are composed of the Asmari limestone. The permeable limbs are mostly surrounded by the Pabdeh-Gorpi impermeable formation. In the western limb

of the monocline a thrust fault with about 10 km lengths, sloping gently in NW-SE direction, while the majority of the medium size faults trending NE-SW is stretched between the Kamarderaz and the Mongasht anticlines (Figure 1).

1.2.1. MONGASHT

The asymmetric fan fold Mongasht anticline trending NE-SW is the largest structure in the area and the Izeh basement fault which caused a change in its trend also resulted in to bend the mid axis. At limbs and hinge line the consolidated carbonate rock is thick and uniform whereas marl and shaly layer thickness are variable and acting as slippery zones. Geometrically, the Mongasht anticline is cylindrical in form and plunging down beneath the younger sediments on both ends. The slope in the eastern part of the anticline is relatively gentle and characterized by NE-SW directing fault lines that overturned the limestone layers resulting to merge the Mongasht and Shavish-Tanosh anticlines. Apart to this fault line, the deep fault systems occurrence in different directions is frequent in many parts of the Mongasht anticline (Figure 1). Remarkable faults (more than 10 km) including the Sepran and the Mongasht thrust are located in the southwestern part of the Mongasht anticline and playing a significant role in groundwater movement and hydraulic connection between the water-bearing horizons like Shavish-Tanosh and Kamarderaz anticlines, and the Naal-e-Asbi. The geological fractures at every scale occurred along with faults and these discontinuities provide the necessary permeability for migration and accumulation of groundwater.

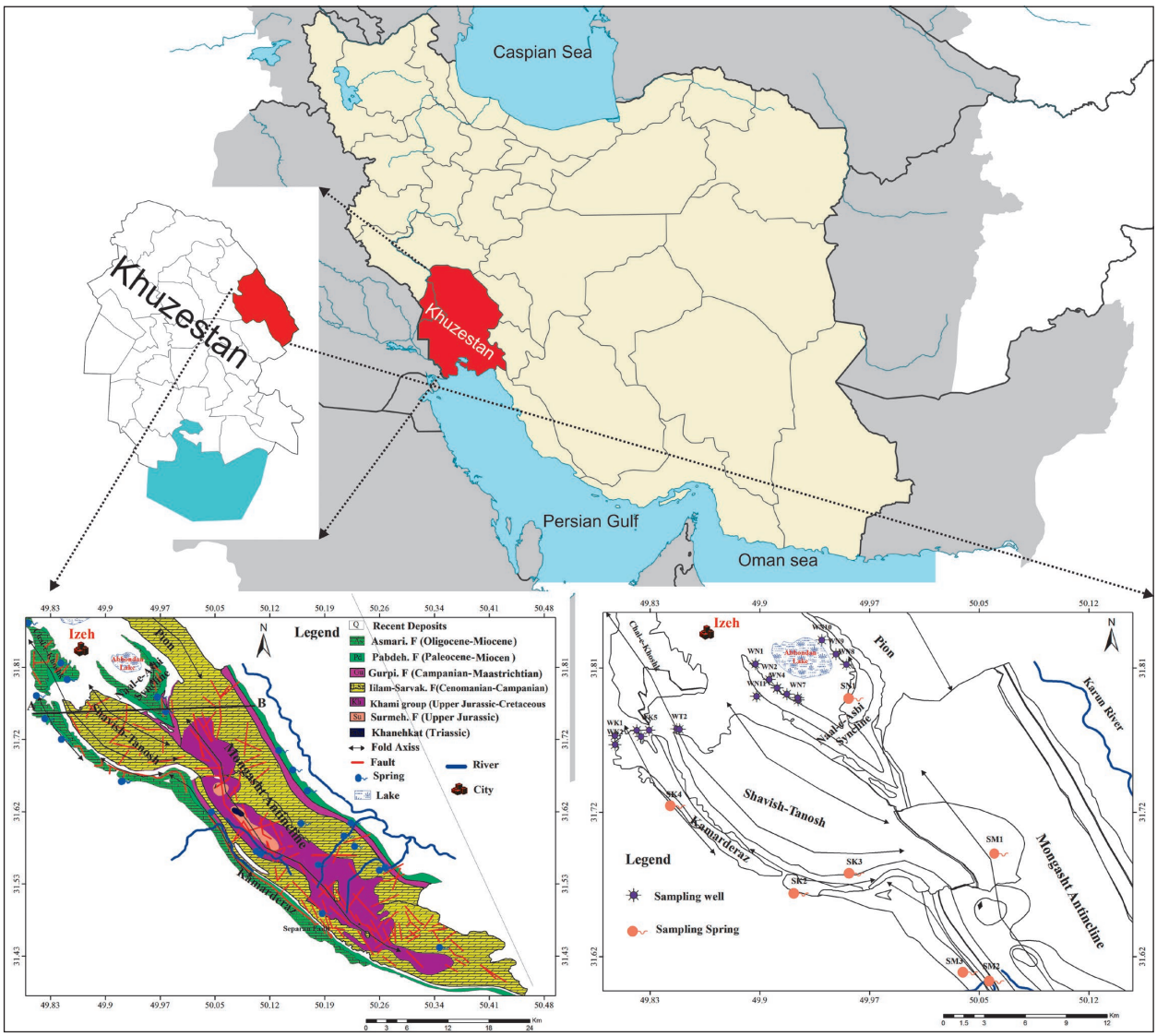

Figure 1: Geological map of the study area and locations of the meteoric water, springs and wells sampling in the Izeh karst catchment.

1.2.2. SHAVISH -TANOSH

The coupled (conjugated) Shavish-Tanosh anticlines directing NW-SE, composed of the Ilam-Sarvak limestone, and the fracture density is moderately more in the eastern limb with respect to the western one.

1.2.3. KAMARDERAZ ANTICLINE

This eroded single-sided anticline with the general trend of northwest-southeast stretches parallel to the Shavish-Tanosh anticline and is composed of the Asmari limestone. The western and eastern sides of the Asmari formation are partly occupied by the impermeable Pabdeh formation. In the southern parts of the anticline, the forces of the tectonic activity have caused the layers to turn. The dominant faults trend is northeast-southwest and there is a thrust fault approximately 10 km long with a slope to the southwest at the northeastern edge of the anticline.

1.2.4. NAAL-E-ASBI SYNCLINORIUM

The Naal-e-Asbi symmetrically folded synclinorium extending 12 km with a width of 2 km in the NW-SE direction and can be divided into north and south sections (Figure 1). This synclinorium is located between the Pion anticline in the north and the Shavish-Tanosh anticline in the south and this is the main and accessible place for groundwater extraction in the Izeh area.

Based on Figure 2, it can be stated that the infiltration of water in the limestone formations of Ilam-Sarvak and Fahlian-Darian in the Mongasht anticline has created a large karst aquifer. The groundwater of the Mongasht karst aquifer flows deep and move through large faults from the Mongasht anticline to the Kamarderaz, Shavish-Tanosh and Chalkhoshk anticlines in the southern parts of the region. Also, the existence of faults and fractures between the Mongasht anticline and the Naal-e-Asbi syncline has caused water to penetrate in to the Naal-e-Asbi syncline.

1.2.5. HYDROGEOLOGY OF IZEH AREA

Morphologically the Izeh plain is an open polje with gentle slopes forming a large lake called as Miangran. The geological formation of the plain which ranges from Upper Cretaceous to the current age consists of heterogeneous alluvial deposits overlying consolidated sedimentary rocks. The Izeh plain has an unconfined groundwater system in unconsolidated sediments while the karstic aquifers occupying the surrounding of the plain composed of massive and highly fractured limestone and dolomite-limestone in a tectonically complex zone. The thickness of the Izeh alluvial sediments ranges from 60 m in the southeast to over 150 m in the northwest. Fine sediments such as silt, clay, and fine sand are deposited underneath the lake at approximately 70 m depth (Alijani, 2003). Most of the Izeh alluvial plain recharge is related to precipitation and the water table depth ranges from 1.5 m to more than 50 m. The annual discharge of the Izeh alluvial plain unconfined aquifer through exploitation wells is about 8.65 Mm^3. Using the absolute water level of the piezometers, water table map of the Izeh plain aquifer for October 2021 was prepared indicating flow direction (Figure 3).

In general, four unconfined karst aquifers are recognized (Figure 2) and playing a significant role concerning drinking water supply of the area. The depth of Izeh area karstic wells varies from 130 to 290 meters and their discharge ranges from 15 to 65 liters per second and the annual discharge is about 19 Mm^3.

The Asmari limestone karstic aquifer contains high storage capacity as well as a dominated base flow and the dolomite Ilam-Sarvak karst in the Shavish-Tanosh anticline is an intermediate aquifer with quick-flow and low storage capacity (Nassery et al., 2013). The characteristics of the dolomite Ilam-Sarvak karst in the Mongasht anticline are similar to the Asmari limestone formation. The karstification of the Asmari formation and the dolomite Ilam-Sarvak karst in the Mongasht resulted in coexisting fracture and conduit flow and unlike the Ilam-Sarvak karst aquifers in the Shavish-Tanosh anticline, the matrix could also easily transmit horizontal flow. The Ilam-Sarvak karst aquifers in the Shavish-Tanosh anticlines lie between two extremes, of low and high karstification and

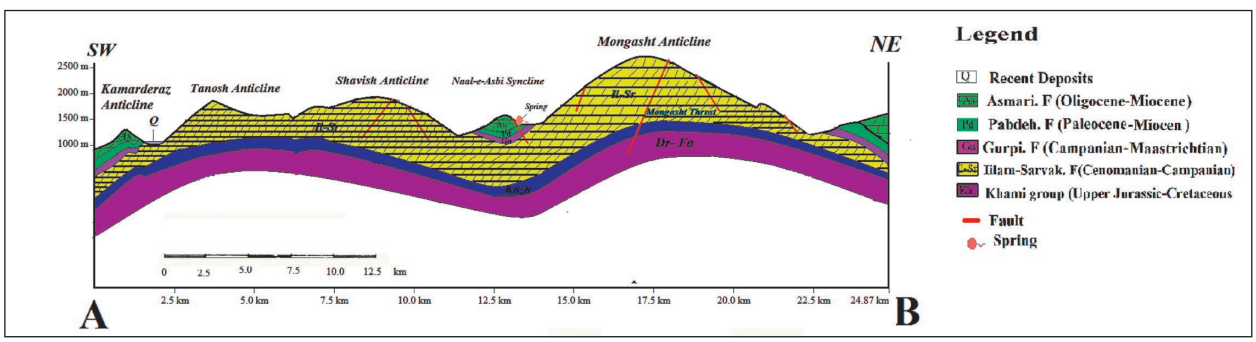

Figure 2: Geological section in the path A-B (Figure 1).

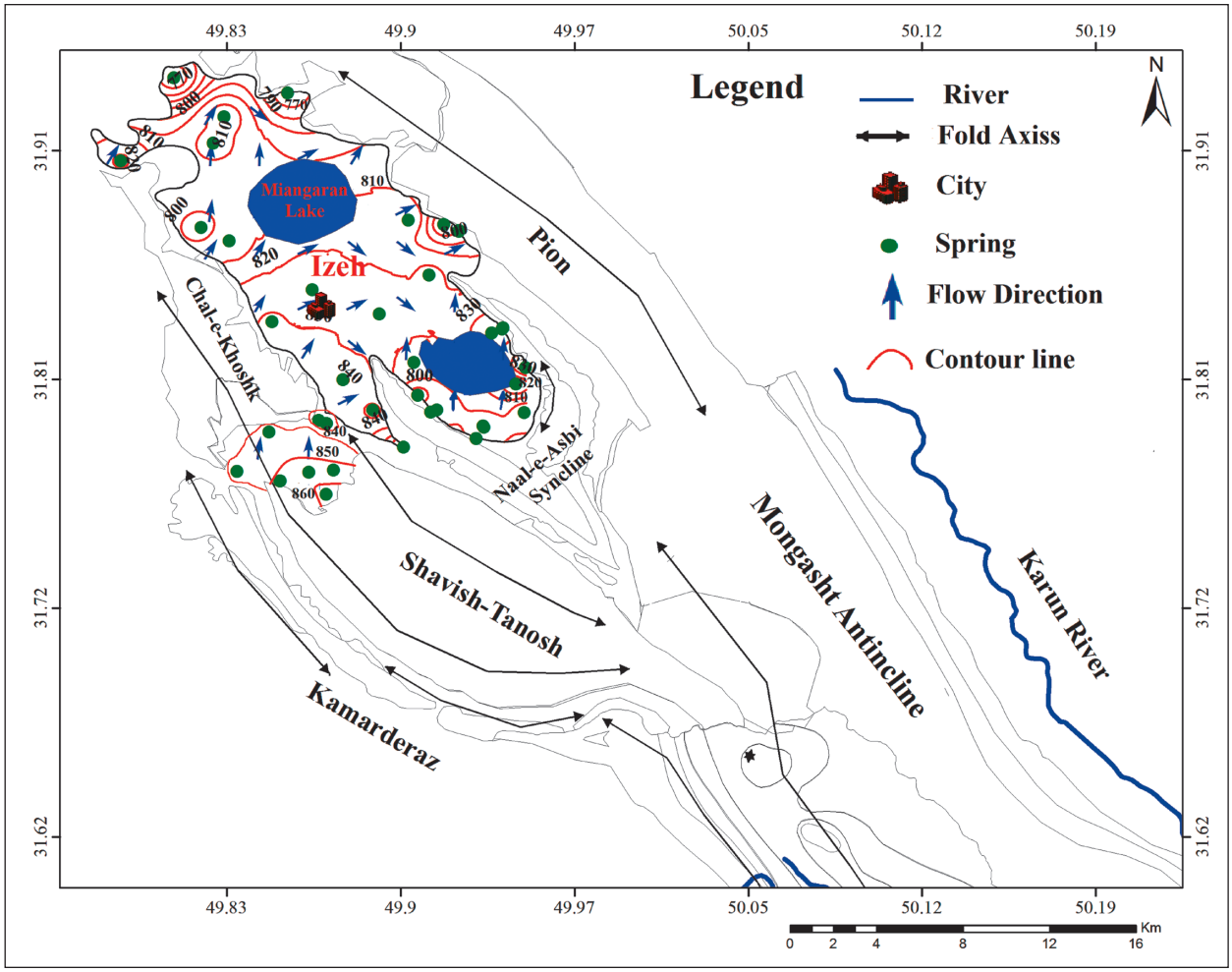

Figure 3: Map of groundwater flow directions of Izeh plain.

thus, the groundwater system is experiencing quick and low base flow.

The limestone complex and the dolomite Ilam-Sarvak karst in the Mongasht anticline exhibits brittle behavior under tectonic stresses, favoring propagation and development of wide fracture networks that are extensively karstified. In the Mongasht complex, groundwater flow is concentrated towards the lower reaches karstic aquifers including; the Shavish-Tanosh and Kamarderaz anticlines, and the Naal-e-Asbi syncline.

In the Izeh area, many low discharge springs (1– 5 L/s) are observed, but from the western limb of the Mongasht anticline a considerable spring (Mal-Agha) emerging out with an annual average discharge of 1.5 m^3 L/s at an elevation of about 2000 m a.s.l (Table 1; Figure 2) The spring is fed by the highly fractured and karstified dolomite rock, which is surrounded by thick sequences of less permeable deposits.

2. MATERIALS AND METHODS

A total 25 groundwater (8 springs and 17 wells) the same locations were sampled twice in January 2020 (wet season) and May 2021(dry season) and 6 rain water samples from selected locations. For evaluation of the stable isotope content of rain water (rainwater samples were sampled from higher altitude feeding areas and lower altitude discharge areas), the main karst springs and wells in the karstic aquifer system, samples were analyzed. The samples were taken from pumping wells and springs across the study area (Figure 1) Water from wells in the area is

extracted using pumps. Physical parameters such as pH, temperature, electrical conductivity, total dissolved solids were measured in situ using standard field equipment such as Mercury in glass thermometer, digital mvRedox pH meter, conductivity meter, WA 3000, and spectrophotometer respectively. Major anions and cations were analyzed using titration, chromatography and flame test in the Zagros Abshenas Laboratory respectively. The trace elements were measured using inductively coupled plasma-mass spectrometry (ICP-OES), using acid digestion method with hydrofluoric acids, sulfuric acid, nitric acid and Perchloric acid in the Zarazma Laboratory. The isoto-

Table 1a: Physico-chemical characteristics of the karst springs and wells in the Izeh area (mg/L). January, 2020.

Name	Location	ID	pH	EC µS/cm	T C°	TDS	Na^+	K^+	Ca^{+2}	Mg^{+2}	HCO_3^-	SO_4^{-2}	Cl^-	Percentage of analysis errors
Abgol (S)	**Mongasht**	**SM_1**	8.2	320	12.8	247.2	1.1	0.4	44.1	9.7	183.1	1.9	7.1	1.44
Malagha1(S)		**SM_2**	8.2	429	12	312.4	1.8	0.4	64.1	10.3	198.3	28.8	8.9	0.01
Malagha2(S)		**SM_3**	8.1	330	11	242.9	1.4	0.4	40.1	12.2	173.9	2.9	12.4	2.87
Takab(S)	**Naal-e-Asbi**	**SN_1**	8.2	278	18	209	3.2	0.4	48.1	1.2	140.3	5.3	10.6	0.49
Kaldozakh		**WN_1**	7.3	707	23	532.7	20.2	1.2	72.1	32.8	366.1	7.2	33.7	3.00
Jamoshi		**WN_2**	7.4	674	22	466.9	19.8	1.2	70.1	29.2	308.1	7.2	31.9	1.08
Lavaii 1		**WN_3**	7.9	377	21	288.2	13.1	0.4	48.1	12.2	195.3	5.3	14.2	0.76
Lavaii 2		**WN_4**	7.5	744	22	521	27.8	1.2	66.1	32.8	335.6	12	46.1	4.64
Bardboran 1		**WN_5**	7.6	471	23	322.7	13.6	0.4	56.1	10.9	216.6	7.7	17.7	3.49
Bardboran 2		**WN_6**	7.5	498	22	373.3	14.7	0.8	63.1	13.9	250.2	4.3	26.6	1.33
Porarshad		**WN_7**	7.6	551	21.5	394.9	16.6	0.8	68.1	16.4	259.3	5.8	28.4	1.07
Abrak		**WN_8**	7.8	469	22.9	314.5	12.2	0.4	52.1	15.8	204.4	8.7	21.3	0.20
Kohbad 1		**WN_9**	7.7	593	23.7	396.1	25.3	1.2	60.1	22.5	195.3	10.6	81.5	3.00
Kobad 2		**WN_{10}**	7.6	582	21.8	382.3	33.3	0.8	58.1	19.4	186.1	19.2	65.6	3.62
Chega		**WN_{11}**	7.4	584	20.5	431.8	11.04	0.8	66.1	25.5	308.1	4.8	15.9	2.21
Tekyeh 1	**Kamarderaz**	**SK_1**	7.2	716	24	548.5	19.1	1.2	86.2	27.9	381.4	19.2	14.2	4.30
Tekyeh 2		**SK_2**	7.8	626	18	478.7	17.7	1.2	64.1	30.4	329.5	24.02	12.4	2.62
Abgorazi		**SK_3**	7.9	782	20.9	554.5	14.7	1.2	109.2	19.4	381.4	9.6	19.5	2.82
Monareh		**SK_4**	8.1	455	22.9	348.3	7.1	0.8	64.1	15.8	238	8.7	14.2	1.96
Number 1 rostaii		**WK_1**	7.7	721	24.6	519.8	55.4	1.6	70.1	18.2	231.9	72.1	70.9	3.29
Number 2 Halayegan		**WK_2**	7.8	542	22.7	387.6	19.1	1.2	50.1	20.7	238	36	23.04	3.75
Number 3 Halayegan		**WK_3**	7.8	451	24.7	353.8	14.7	0.8	52.1	17	231.9	28.8	8.9	1.01
Number 4 Halayegan		**WK_4**	7.8	528	23.2	388.3	26.2	1.2	60.1	13.4	222.7	38.4	26.6	2.33
Number 5 Tangsofla	**Shavish-Tanosh**	**WT_1**	7.6	500	23.7	398.4	11.9	1.2	70.1	18.2	280.7	9.6	7.09	0.09
Number 6 Tangoliya		**WT_2**	7.6	500	23.7	404.4	12.6	1.2	88.2	7.3	274.6	12	8.9	0.67
AVR			**7.73**	**537.12**	**20.70**	**392.73**	**16.55**	**0.90**	**63.63**	**18.12**	**253.23**	**15.60**	**25.11**	**2.08**
MAX			**8.20**	**782.00**	**24.70**	**554.50**	**55.40**	**1.60**	**109.2**	**32.8**	**381.40**	**72.1**	**81.5**	**4.64**
MIN			**7.2**	**278.0**	**11**	**209.0**	**1.1**	**0.4**	**40.1**	**1.2**	**140.3**	**1.9**	**7.09**	**0.01**

pic samples (30 samples in two seasons (6 rainwater samples in January 2020, 7 spring samples and 17 well samples in two seasons, table 4) were analyzed for δ^2H and $\delta^{18}O$ values with precision ±0.1‰ for $\delta^{18}O$ and ±1‰ for δ^2H in the Mesbah Energy Laboratory of Arak with the use of Off- Axis-integrated- Cavity- Output- Spectroscopy (OA-ICOS). Stable isotope ratios are reported in parts per mille (‰) using the conventional delta notation. For hydrochemical interpretation and to get knowledge about the hydraulic connection between karstified and water bearing structures various graphs, including, Gibbs (1970) and Langelier and Ludwig (1942) were taken into account.

Table 1b: Physico-chemical characteristics of the karst springs and wells in the Izeh area (mg/L). May 2021.

Name	Location	ID	pH	EC µS/cm	T C°	TDS	Na^+	K^+	Ca^{+2}	Mg^{+2}	HCO_3^-	SO_4^{-2}	Cl^-	Percentage of analysis errors
Abgol	**Mongasht**	**SM_1**	8.3	320	13.3	234.3	0.91	0.39	50.1	7.9	140.3	21. 3	1.8	2.8
Malagha1		**SM_2**	8.3	343	15	242.8	0.91	0.4	44	14.5	140.3	23.1	1.8	2.8
Malagha2		**SM_3**	8.2	408	12	298.5	1.1	0.8	53.1	16.4	195.3	14.9	5.3	3.01
Takab	**Naal-e-Asbi**	**SN_1**	8.1	287	20	455	3.8	1.6	64.1	39.5	292.9	42.3	63.8	3.1
Kaldozakh		**WN_1**	7.4	781	25	527.1	23.6	1.5	60.1	34.6	299	52.8	30.1	3.2
Jamoshi		**WN_2**	7.5	675	24	498.3	20.7	1.6	80.1	28.5	305.1	40.8	42.5	2.8
Lavaii 1		**WN_3**	7.8	713	23	526.4	28.3	1.2	68.1	19.4	268.5	40.8	15.9	3.1
Lavaii 2		**WN_4**	7.6	584	25	430.8	17.2	1.5	60.1	32.2	305.1	48.03	30.1	3.1
Bardboran 1		**WN_5**	7.7	689	25	503.9	27.4	0.7	60.1	15.8	247.1	9.6	8.8	3.2
Bardboran 2		**WN_6**	7.7	452	26	346.7	4.8	1.1	56.1	29.2	292.9	32.2	14.2	3.3
Porarshad		**WN_7**	7.5	580	27	440.7	15.6	1.6	76.1	32.8	274.6	31.2	99.3	2.7
Abrak		**WN_8**	7.5	785	25.9	550.4	35.4	1.5	90.1	18.2	244.1	38.4	106.4	2.3
Kohbad 1		**WN_9**	7.6	785	26.5	552.9	54.4	1.9	80.1	45.5	213.6	156.1	124.1	2.3
Kobad 2		**WN_{10}**	7.7	1021	24.5	703.7	82.9	1.9	90.1	42.5	210.5	180.1	120.5	2.2
Chega		**WN_{11}**	7.5	1121	23.5	733.8	88.7	1.5	40.0	63.1	305.1	88.9	88.6	3.5
Tekyeh 1	**Kamarderaz**	**SK_1**	7.5	741	25	514.9	8.27	4.3	80.2	26.7	198.3	24.02	28.4	1.9
Tekyeh 2		**SK_2**	7.7	759	19	1376.	16.09	1.17	60.1	21.3	274.6	12.01	5.3	3.4
Abgorazi		**SK_3**	7.6	496	22.9	377.2	3.219	2.7	80.1	42.5	180	216.1	184.4	2.2
Monareh		**SK_4**	7.6	476	23.9	387.6	8.1	1.9	70.1	36.4	201.4	170.5	54.9	2.4
Number 1 rostaii		**WK_1**	7.5	1264	26.6	839.1	23.8	1.2	60.1	21.9	161.7	88.9	26.6	2.5
Number 2 Halayegan		**WK_2**	7.4	864	27.7	614.3	37.5	1.3	52.1	24.3	195.3	92.7	19.5	2.9
Number 3 Halayegan		**WK_3**	7.7	561	28.8	385.6	25.7	1.4	60.1	13.4	222.7	38.4	26.6	2.8
Number 4 Halayegan		**WK_4**	7.6	565	26.3	411.2	26.6	1.1	65.1	28.5	265.4	24.9	8.8	3.4
Number 5 Tangsofla	**Shavish-Tanosh**	**WT_1**	7.5	520	26.4	384.5	5.9	1.27	50.1	30.4	259.3	36.5	8.8	3.4
Number 6 Tangoliya		**WT_2**	7.4	527	25.8	391.5	5.7	1.3	50.1	31.9	140.3	21.1	1.7	2.7
AVR			**7.7**	**652.6**	**23.5**	**509.2**	**23.4**	**1.5**	**64.1**	**28.7**	**233.3**	**61.8**	**41.5**	**2.8**
MAX			**8.3**	**1264**	**28.8**	**1376.9**	**88.7**	**4.3**	**90.1**	**63.1**	**305.1**	**216.1**	**184.4**	**3.5**
MIN			**7.4**	**287**	**12**	**234.3**	**0.9**	**0.3**	**40**	**7.9**	**140.3**	**9.6**	**1.8**	**1.9**

3. RESULTS AND DISCUSSION

3.1. HYDROCHEMICAL CHARACTERISTICS

The hydrochemical properties of groundwater samples for two seasons (wet and dry) are shown in Tables 1a and 1b, and the chemical ionic balance is also presented. The pH of groundwater samples is slightly alkaline and varies from 7.18 to 8.22. The temperature varies from 12.8 °C to 24.8 °C with a mean value of 19 °C. The EC and TDS of the groundwater samples varying from 278 to 1325 µS/cm and 209 to 944 mg/L respectively. The rise of EC in wells WN_1, WN_2 and WN_4 located in the Naal-e-Asbi can be considered as a result of reversing groundwater flow direction from the alluvial aquifer into the Naal-e-Asbi karstic aquifer. Reversing the flow direction is due to recent droughts and excessive water abstraction from the calcareous aquifer, which caused the karstic aquifer water level to recede with respect to the alluvial aquifer (Kalantari et al., 2009).

There are low differences in water temperatures and

Table 2: Information's about groundwater sources, containing wells and springs.

Name	Location	ID	Altitude	Well depth	Discharge
			m	m	L/s
Abgol (Spring)	**Mongasht**	**SM_1**	1041	-	6
Malagha1 (Spring)		**SM_2**	2238	-	2/4
Malagha2 (Spring)		**SM_3**	2218	-	2/2
Takab (Spring)	**Naal-e-Asbi**	**SN_1**	989	-	1
Kaldozakh		**WN_1**	841	180	30
Jamoshi		**WN_2**	861	240	35
Lavaii 1		**WN_3**	838	260	37
Lavaii 2		**WN_4**	838	230	30
Bardboran 1		**WN_5**	942	180	9.8
Bardboran 2		**WN_6**	857	200	32
Porarshad		**WN_7**	841	150	12
Abrak		**WN_8**	883	150	50
Kohbad 1		**WN_9**	838	130	62
Kobad 2		**WN_{10}**	840	220	50
Chega		**WN_{11}**	900	150	30
Tekyeh 1 (Spring)	**Kamarderaz**	**SK_1**	1041	-	0/5
Tekyeh 2 (Spring)		**SK_2**	1038	-	0/1
Abgorazi (Spring)		**SK_3**	1143	-	0/2
Monareh (Spring)		**SK_4**	916	-	0/8
Number 1 rostaii		**WK_1**	858	90	40
Number 2 Halayegan		**WK_2**	861	110	15
Number 3 Halayegan		**WK_3**	856	120	46
Number 4 Halayegan		**WK_4**	855	120	30
Number 5 Tangsofla	**Shavish-Tanosh**	**WT_1**	855	150	65
Number 6 Tangoliya		**WT_2**	850	220	15

EC change in the wet and dry seasons. The concentration of SO_4^{-2} ion placed between 1.9 mg/L to 72.1 mg/L with an average of 15.6 mg/L, and the highest and lowest sulfate concentration was observed in the well sample (WK_1) and SM_1 and SM_2 springs respectively.

The data concerning the karstic wells depth, altitude and discharge rate and the springs discharge and altitude is given in Table 2. The wells depth varies from 90 to 260 meters and their discharge rate ranges from 15 to 65 L/s. The annual abstraction from the Izeh karst aquifers for drinking is 18.65 Mm^3. Of course there is a difference in water usage in the wet (5,927 Mm^3) and dry (12,723, Mm^3) seasons.

The location of the samples in the Durov diagram (Figures 4a-b) indicates that wells and springs are dominantly from similar geological units comprising of the Asmari limestone (Oligocene to Miocene) and the Ilam-Sarvak limestone-dolomite (Upper Cretaceous). The Durov plot for groundwater samples indicates that most of the samples are in the phase of mixing dissolution.

Increasing Cl^- can be attributed to the dissolution of halite in alluvium and the reversal of the flow from the Izeh aquifer to the kartic aquifer (Srivastava & Ramanathan, 2008).

3.1.1. HYDROCHEMICAL PROCESSES

The binary diagrams of the major elements (Figure 5) confirm that dissolution and water-rock interactions are the dominant factors to control groundwater chemistry. Based on the comparison between Ca^{+2} vs. HCO_3^-, Mg^{+2} vs. HCO_3^- and Ca^{+2} vs. Mg^{+2} (Figures 5a-c), it seems that there is a notable difference in the kinetic of calcite and dolomite dissolution. Two different processes occur successively; first, a congruent dissolution of calcite with marginal contribution of dolomite until saturation with respect to calcite and its subsequent precipitation and

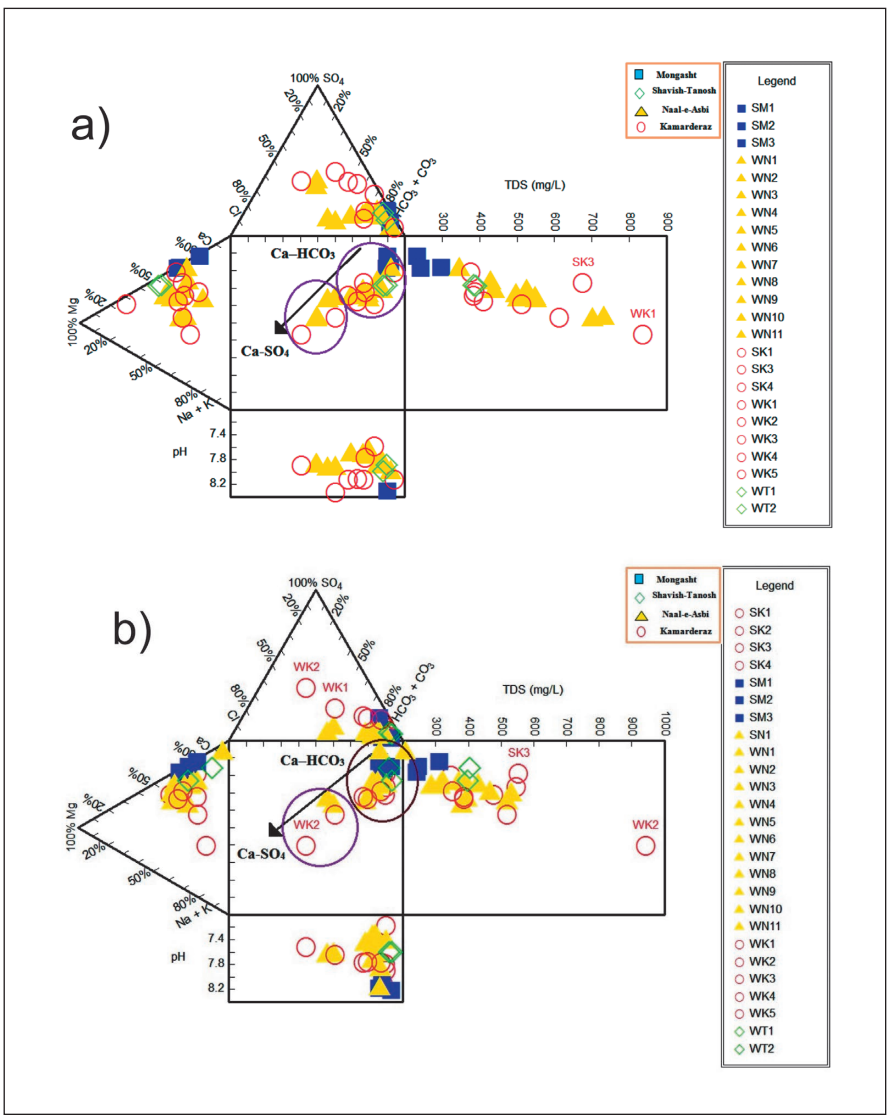

Figure 4: Durov plot of chemical analysis of the groundwater samples, wet season (a) and dry season (b).

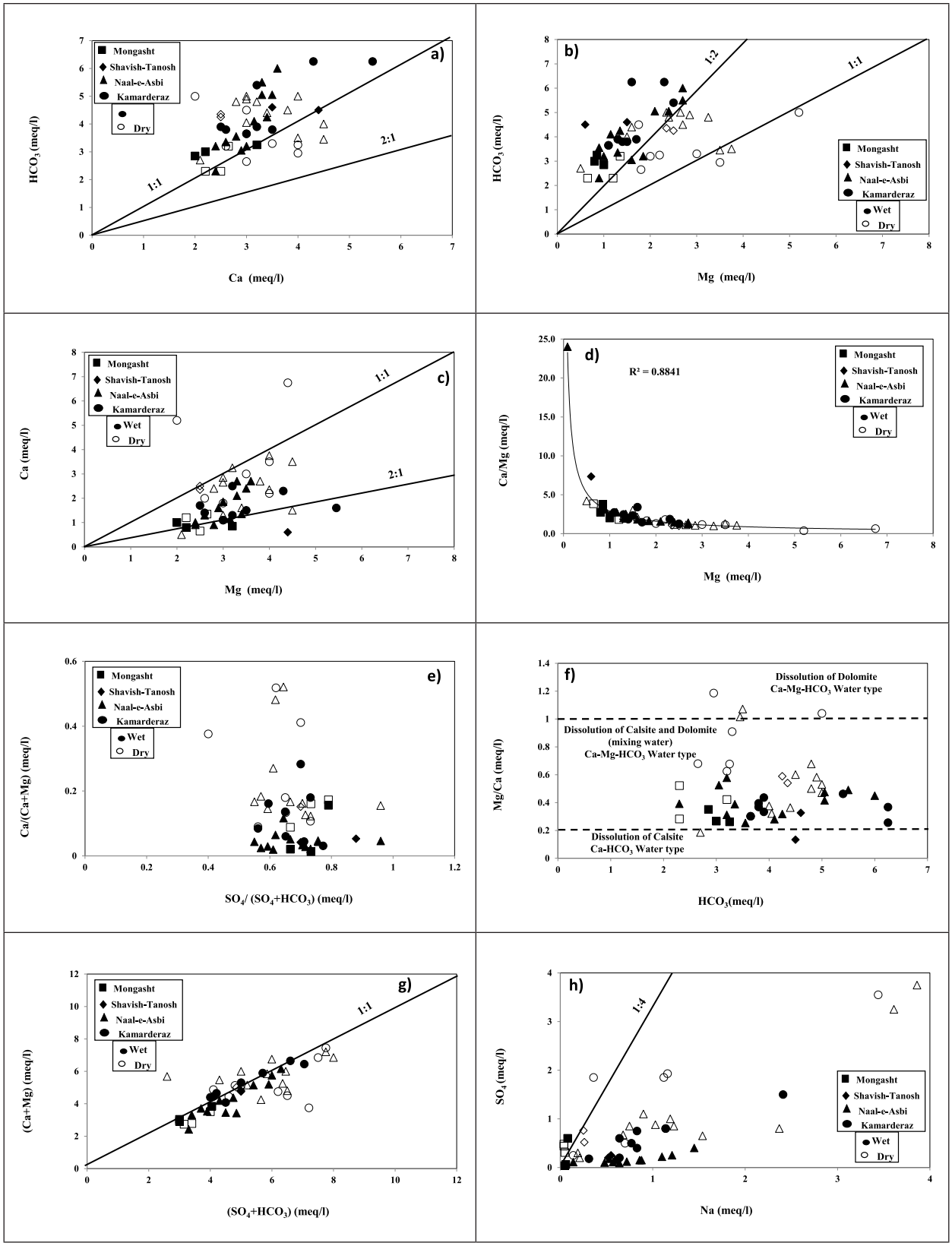

Figure 5: Plot of Ca^{+2} vs. HCO_3^- (a), Mg^{+2} vs. HCO_3^- (b), Ca^{2+} vs. Mg^{2+} (c), Ca^{2+}/Mg^{2+} vs. Mg (d), $Ca^{2+}/Ca^{2+} + Mg^{2+}$ vs. $SO_4^{2-}/SO_4^{2-} + HCO_3^-$ (e), $Ca^{2+} + Mg^{2+}$ vs. HCO_3^- (f), $Ca^{2+} + Mg^{2+}$ vs. $SO_4^{2-} + HCO_3^-$ (g) and Na^+ vs. SO_4^{2-} for the groundwater samples (h).

second, an incongruent dissolution of dolomite (Celle-Jeanton et al., 2001; Emblanch, 2003). The dedolomitization induces a gradual enrichment in magnesium and gradual depletion of calcium (Figure 5c) related to affect of rocks porosity and density (Nader et al., 2003; Ren & Jones, 2017; Makhloufi et al., 2018).

The composition of the karstic water systems is due to dissolution of variable quantities of calcite and dolomite. The proportion of calcite and dolomite in an aquifer is, together with the transit time, one of the basic factors influencing the chemical composition of karstic waters. Hence, the Mg^{+2}/Ca^{+2} ratios are often used as a good indicator of residence time. Calcite dissolves more quickly than dolomite and shows a rapid equilibrium with the hosted rock while Mg^{+2} concentrations reveal a progressive increase with flow paths and residency (Figure 5d). More evolved water in the Kamarderaz anticline and the Naal-e-Asbi has higher temperature, magnesium content and Mg^{2+}/Ca^{2+} ratio; therefore, these parameters can be utilized as indicators of the degree of hydrochemical evolution. In addition, a good correlation between water temperature and magnesium concentration or Mg^{+2}/Ca^{+2} ratios indicates that an increase in temperature accelerates the kinetics of the dissolution of dolomite. The higher temperatures tend to accelerate the kinetics of the dolomite dissolution reaction (Moral et al., 2008).

Also in the $Ca^{2+}/Ca^{2+}+Mg^{2+}$ vs. $SO_4^{2-}/SO_4^{2-}+HCO_3^-$ in Figure 5e, high values of $Ca^{2+}/Ca^{2+}+Mg^{2+}$ indicate the predominant reaction of water with calcite. However, if the water reacts with dolomite, samples position should be in the middle areas of the Figure 5e.

The plot of Mg^{2+}/Ca^{2+} vs. HCO_3, (Figure 5f) used to determine the possible sources of Ca^{2+} and Mg^{2+} ions in groundwater. It is evident from the $Ca^{2+}+Mg^{2+}$ vs. HCO_3^-, that most of the samples fall between the line 0.2 and 1. The Mg^{2+}/Ca^{2+} molar ratios of the groundwater samples were in the range 0.04 to 0.8 (average: 0.48). As shown in Figure 5f, the Ca^{2+} concentration in groundwater is mainly controlled by dissolution of calcite and dolomite. This plot reflecting extra sources of HCO_3^- ion in the Naal-e-Asbi and Kamarderaz samples, indicating that the calcium carbonate weathering (Asmari formation) it has not sufficient HCO_3^- to explain the concentrations. The additional amounts of HCO_3 must be supplied from the upper reaches Ilam-Sarvak limestone-dolomite formation.

Binary plot of $Ca^{2+}+Mg^{2+}$ vs. SO_4^{-2} + HCO_3^- (Figure 5g) in study area shows that most of the samples fall around the 1:1 line which indicates that dissolution of calcite, dolomite and gypsum are the dominant reactions in the system (Zaidi et al., 2015). Extra amounts of Ca^{2+} + Mg^{2+} over SO_4^{2-} +HCO_3^- indicate the ion exchange process, while excess amounts of SO_4^{2-} +HCO_3^- over Ca^{2+} +Mg^{2+} show occurrence of reverse ion exchange (Hounslow, 1995; Zaidi et al., 2015; Badaruddin et al., 2017; Alfarrah & Walraevens, 2018). As shown in Figure 5g, all of the samples spread on the 1:1 line of ($Ca^{2+}+Mg^{2+}$) and ($HCO_3^-+SO_4^{2-}$), depicting the crucial role of the carbonate dissolution. The sample numbers WN_2, WN_9, and WN_{10} show deviation from this line indicating the presence of reverse ion exchange (Rajmohan & Elango, 2004). An excess of $Ca^{2+}+Mg^{2+}$ over $SO_4^{2-}+HCO_3^-$ may be due to exchange of sodium in water with calcium and magnesium. Increased sodium is due to the reversal of flow direction from the surrounding alluvial aquifers and mixing phenomena.

Enrichment of Na^+, Mg^{2+} and SO_4^{2-}, water samples with linear correlation of the SO_4^{2-} and Na^+ (Figure 5h) indicates weathering and dissolution of Mg^{2+} bearing minerals (Zhou et al., 2016), which could be related to the higher altitude of the Ilam-Sarvak formation with respect to the carbonate formations in the catchment areas of the springs and wells.

Thus, the main geochemical processes in the Izeh karstic aquifers are dissolution of CO_2 and calcite, incongruent dissolution of dolomite, dedolomitization, precipitation of calcite and magnesium enrichment in groundwater.

3.2. HYDRAULIC CONNECTION ASSESSMENT USING MAJOR AND TRACE ELEMENTS

Figure 6 shows the general direction of karst flow in the area. Thus, according to the topography of the area, the height decreases from the Mongasht anticline to other structures. Existence of Izeh and Thrust Mongasht foundations, as well as faults and longitudinal and transverse fractures in these structures cause hydraulic connection between these structures.

Major and minor elements have been extensively used to ascertain geochemical processes and water resource deterioration, and it is also a tool to determine interconnection between different water bodies (Zhang et al., 2020; Ciner et al., 2021; Jiang et al., 2021; Lewinska-Preis et al., 2021; Pratama et al., 2021; Tang et al., 2021).

In the present study, to support the major ions evidences, the trace elements have been also considered to trace groundwater flow between karstic aquifers in the area. In order to recognize the minor elements, samples were analyzed for Al^{+3}, As^{+3}, Ba^{+2}, Cr^{+2}, Li^{+2}, Mo^{+2}, S^{+4}, Si^{+2}, Sr^{+2} and Zn^{+2}. Generally, the trace element concentrations in karst water are low and are not always detectable. The measured values of the minor elements in the karstic aquifers show in Table 3:

The ionic values of groundwater samples suggested that the chemical evolution of groundwater was mainly related to the geogenic process and recharge water.

Table 3: Descriptive table (min, max, avr) heavy metals of groundwater samples in the study area (N = 25).

Elements	Al^{+3}	As^{+3}	Ba^{+2}	Cr^{+2}	Li^{+2}	Mo^{+2}	S^{+4}	Si^{+2}	Sr^{+2}	Zn^{+2}
Minimum	11	120	7.8	1200	1.1	0.21	1600	2030	150	1.12
Maximum	180	6500	208	2400	17.8	4.4	61360	9220	4090	293
Avr	20	80	50	500	6	0.1	13100	6200	1600	20

Therefore, in accordance with correlation matrix, major ions ratios and the relationship of major ions and some heavy metals such as Li^{+2}, Sr^{+2}, Ba^{+2}, Zn^{+2}, Cr^{+2}, Mo^{+2}, Si^{+2} were used to designate common origin of water, hydraulic interrelationship and groundwater exchange between the karstic aquifers in the command area. Heavy metals that play a key role in determining the origin of calcite water and are present in the region.

The Pearson correlation matrix (Table 4) was used to assess the relationships between the hydrochemical parameters and to disclose recharge sources of different elements. When the correlation coefficient (r) is greater than 0.7, parameters are viewed to be firmly correlated, while if the r value is between 0.5 and 0.7, it depicts a moderate to noteworthy level of correlation (Rudy et al., 2020).

The negative correlation of EC with pH implies their inverse relationship in dissolution processes, and demonstrating enhancing decomposition of soluble materials with decreasing pH and acidity. Negative pH correlation with other ions is attributed to the high corrosion of the acidic environment relative to the soil and host rock, which increases the concentration of ions further (Helena et al., 2000).

P-Value "probability with meaning" or Sig helps us to decide whether or not to reject the null hypothesis without referring to tables of statistical distributions. According to the Sig values in Table 4, it can be said that there is the highest probability of correlation between the elements Ca^{+2}, Mg^{+2}, HCO_3^- and Sr^{+2}.

There is a high relationship between EC and Ca^{+2} (0.81), Mg^{+2} (0.67), and HCO_3^- (0.88), indicating calcite and dolomite origin of aquifers. The strong positive correlation between the sodium and chloride can be attributed to the dissolution of halite in the alluvium and the reversal of the flow from the alluvial aquifers to the karstic aquifer in the region (Srivastava & Ramanathan, 2008). Based on Figure 7, there is a linear trend between the ratios of Ca^{+2}/Zn^{+2} and Mg^{+2}/Zn^{+2}, which indicates the common origin of these ions (calcareous formations), and interrelationship of the samples.

In karstic areas, dissolution of carbonate rocks leads to the entry of Ca^{+2}, Mg^{+2} and Sr^{+2} in groundwater. The increasing trend of Sr^{+2} ion in the samples close to the calcite formations (Naal-e-Asbi and Kamarderaz) in comparison to concentration of Sr^{+2} in dolomite formations (Mongasht and Shavish-Tanosh anticlines), reveals the probable groundwater flow from the Mongasht anticline to the Shavish-Tanosh, Kamarderaz anticlines and Naal-e-Asbi, and the hydraulic relationship between these structures. Recharge from Shavish-Tanosh dolomitic formation has caused the amount of Sr^{+2} in samples WN_5, WN_6, WN_7 to be less than the calcareous formations samples (Figure 8a).

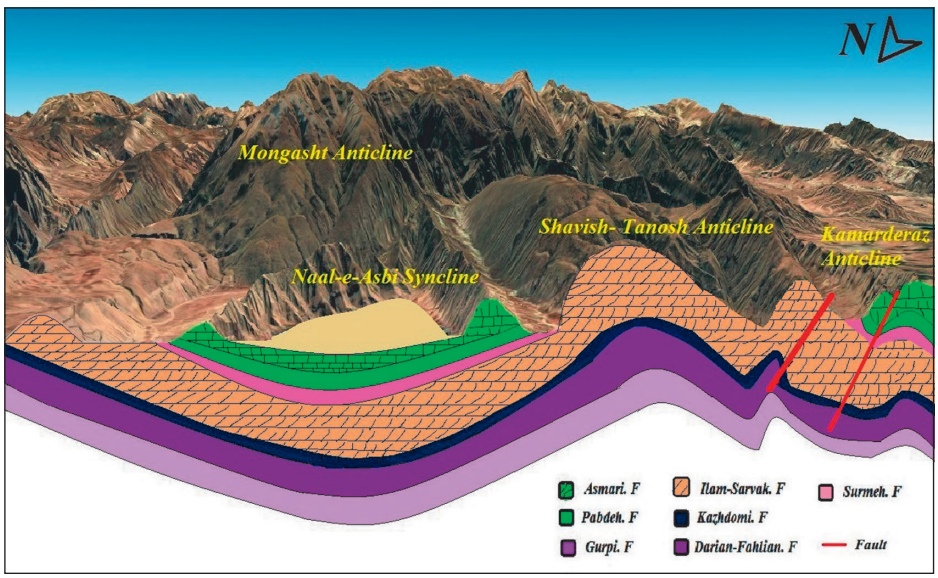

Figure 6: A cross-section of the Mongasht, Shavish-Tanosh, Kamarderaz and Naal-e-Asbi, which shows the merging of these anticlines.

Table 4: Correlation matrix of the trace elements in groundwater samples.

	EC	pH	Ba^{+2}	Cr^{+2}	Li^{+2}	Mo^{+2}	Si^{+2}	Sr^{+2}	Zn^{+2}	Ca^{+2}	Mg^{+2}	Na^{+}	K^{+}	HCO_3^{-}	SO_4^{-2}	Cl^{-}
EC	1															
pH	0.7	1														
Ba^{+2}	**0.74**	-0.48	1													
Cr^{+2}	0.39	-0.39	0.45	1												
Li^{+2}	**0.76**	-0.8	**0.77**	**0.55**	1											
Mo^{+2}	**0.48**	-0.52	0.31	0.22	**0.79**	1										
Si^{+2}	**0.72**	-0.66	-0.09	-0.33	0.07	0.28										
Sr^{+2}	0.31	-0.38	**0.64**	0.37	0.68	0.47	1									
Zn^{+2}	-0.27	0.26	0.25	**0.48**	**0.51**	0.43	0.26	1								
Ca^{+2}	**0.73**	-0.45	-0.16	-0.14	-0.28	-0.21	-0.41	-0.34	1							
Mg^{+2}	**0.81**	-0.74	0.74	0.27	**0.58**	0.42	**0.57**	-0.03	-0.25	1						
Na^{+}	0.67	-0.51	0.68	0.43	**0.81**	0.51	**0.66**	0.46	-0.15	0.35	1					
K^{+}	**0.8**	-0.59	0.11	0.06	0.3	0.19	0.45	0.33	-0.23	0.24	0.44	1				
HCO_3^{-}	**0.8**	-0.6	**0.5**	0.08	**0.51**	0.42	**0.64**	0.16	-0.23	**0.62**	**0.59**	**0.71**	1			
SO_4^{-2}	0.29	-0.04	**0.89**	0.47	**0.87**	**0.62**	**0.71**	0.24	-0.16	**0.79**	**0.74**	0.19	**0.62**	1		
Cl^{-}	**0.5**	-0.3	-0.14	-0.36	-0.03	0.19	0.07	0.07	-0.19	0.07	0.04	**0.69**	0.49	-0.07	1	
Sig.	0.25	**0.54**	0.01	0.02	0.16	0.12	0.05	0.47	0	0.47	0.95	0.001	0.03	**0.58**	0.01	0.01

Also by using the ratios of Ca^{+2}/Sr^{+2} and Mg^{+2}/Sr^{+2} the origin of karst waters can be determined (Negrel & Petelet-Giraud, 2005). Figure 8b shows the very close relationship of Ca^{+2}/Sr^{+2} and Mg^{+2}/Sr^{+2} ratio in the karst groundwater of the region and the common origin of these elements (r^2=0.83). Of course samples originating from the calcareous formations (Asmari) have lower Mg^{+2}/Sr^{+2} ratios than the samples from the dolomitic-calcareous formations (Ilam-Sarvak).

The significant linear positive correlation between Sr^{2+}/Ca^{+2} and Sr^{2+}/HCO_3^{-} indicates dissolution of calcium bearing minerals producing Sr^{2+}in the karstic aquifers

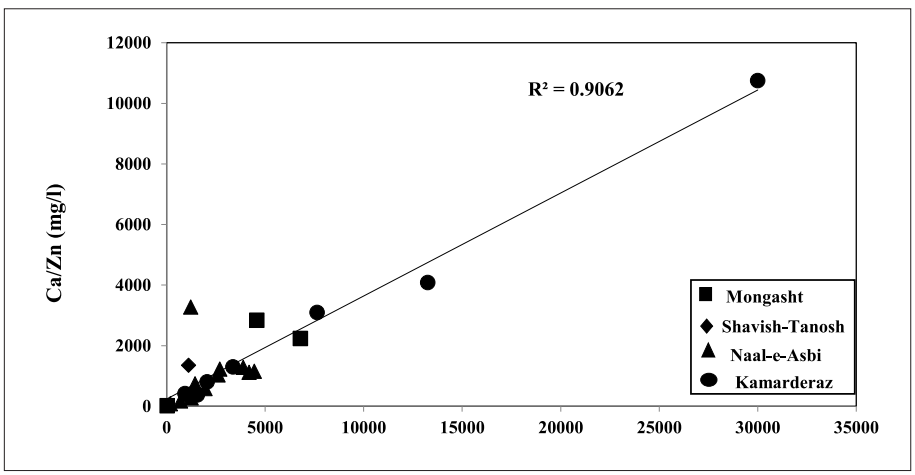

Figure 7: The covariation of Ca^{+2} / Zn^{+2} vs. Mg^{+2} / Zn^{+2}.

(Figure 8c). Furthermore, there is a significant positive correlation between Ca^{2+}, Mg^{2+}, HCO_3^- and Sr^{2+} (Figures 8 a-c), which reflects that the changes of Sr^{2+} as well as Ca^{2+} and Mg^{2+} concentrations in groundwater are caused by calcite and calcite- dolomite dissolution in groundwater. These negative and positive correlations between the variables indicate governing factors controlling hydrochemical process, evolution of groundwater and common origin of ions.

Because the dolomite rocks have more magnesium and less barium than the calcite rocks, groundwater from the calcareous formations has relatively low Mg^{+2} and more Ba^{+2} than the dolomite rocks (Fairchild et al., 2000).

According to the above, the springs and wells dolomitic (SM_1, SM_2, SM_3, WT_1, WT_2) have less ratio Mg^{+2}/Ba^{+2} vs Ca^{+2}/Ba^{+2} (Figure 9a) than samples of calcite (WK, WN). Due to the water flow due to the topography of from the Mongasht anticline to others structure (Naal-e-Asbi, Shavish-Tanosh and Kamarderaz), the water mixing of these structures has brought the values of this ratio and linear process (water mixing).

Figure 9b show clearly liner trends in the distribution of the samples pertaining to the Mg^{+2} vs. Ba^{+2} ratio. The increasing trends of the ion ratios from the Mongasht anticline (SM_1, SM_2, and SM_3) to the Shavish-Tanosh (WT_1, WT_2), Kamarderaz (WK) and Naal-e-Asbi (WN) structures prove their hydraulic connection.

To better understand the relationship between the structures of the region, in this section, the northern and southern limbs of the Naal-e-Asbi syncline are discussed separately. The northern limb of the Naal-e-Asbi navigator is close to the Mongasht anticline and the southern limb of this syncline is close to the Shavish-Tanosh anticline. Therefore, it is assumed that the northern limb is by the Mongasht anticline. The southern limb is also affected by mixed waters of Shavish-Tanosh and alluvium.

In addition to correlation coefficient assessment of the major and trace elements, another approach, including plot of the major elements (Ca^{+2}, Mg^{+2} and HCO_3^-) with trace elements (Li^{+2}, Cr^{+2}, Mo^{+2}) and trace elements with each other was undertaken. The results indicated that samples of different locations; except the southern nose of the Naal-e-Asbi and one or two from the Kamarderaz anticline which are partly recharging from the

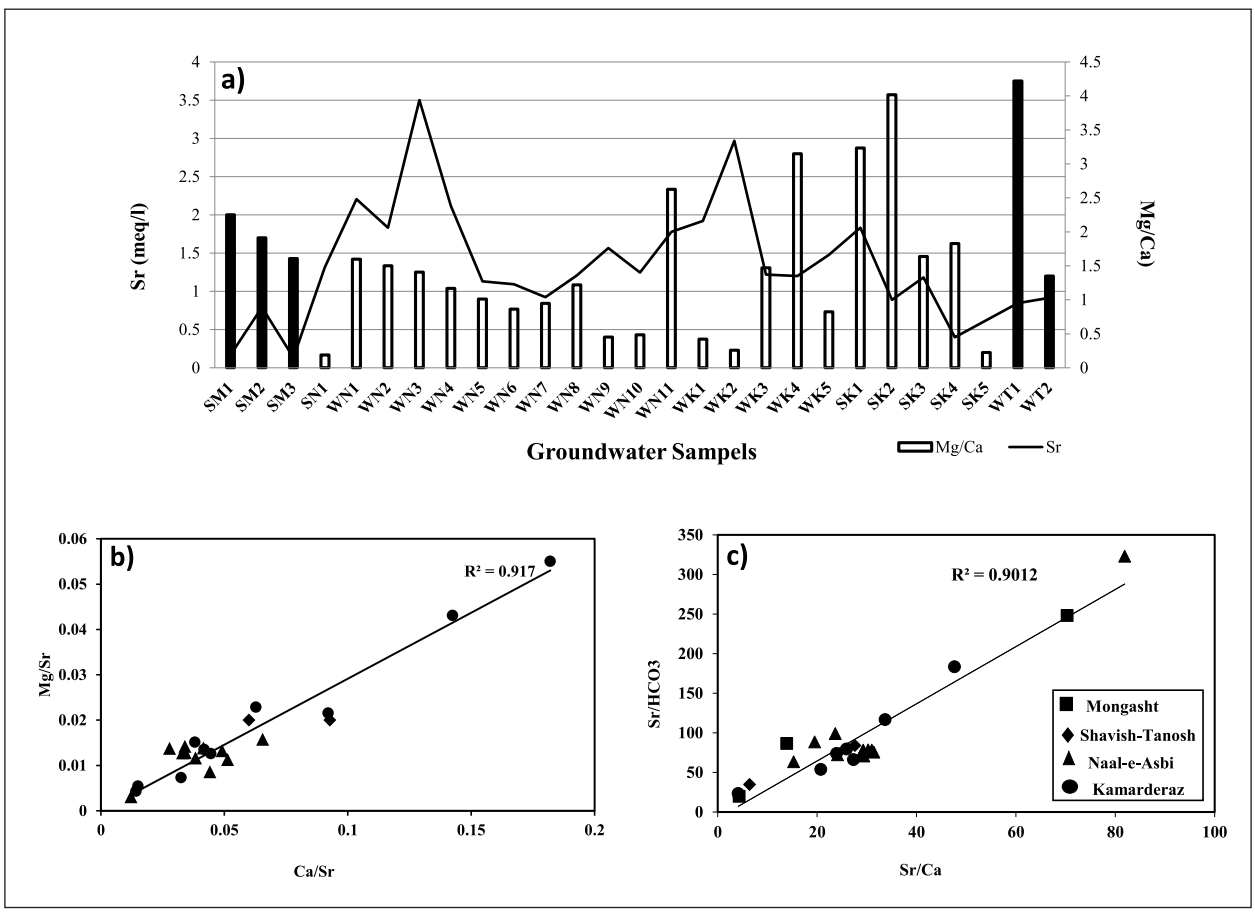

Figure 8: The value of Mg^{+2}/Ca^{+2} and Sr^{+2} (a), Ca^{+2} / Sr^{+2} vs. Mg^{+2} /Sr^{+2} (b), Sr^{+2}/HCO_3^- vs. Sr^{+2}/Ca^{+2} (c) in groundwater structures of the region

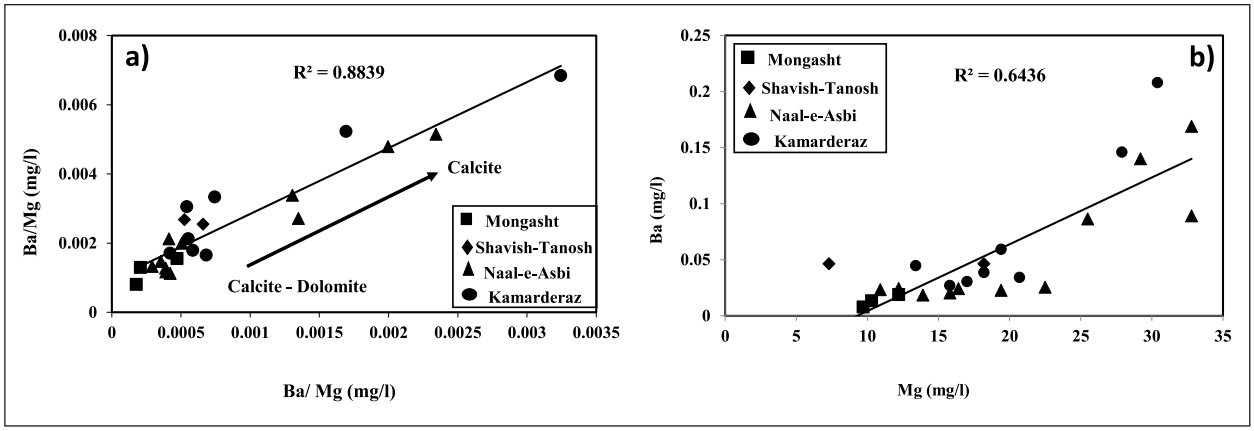

Figure 9: The covariation of Ba^{+2}/ Mg^{+2}vs Ba^{+2}/Ca^{+2} (a) and Ba^{+2} vs. Mg^{+2} (b) in groundwater of the area.

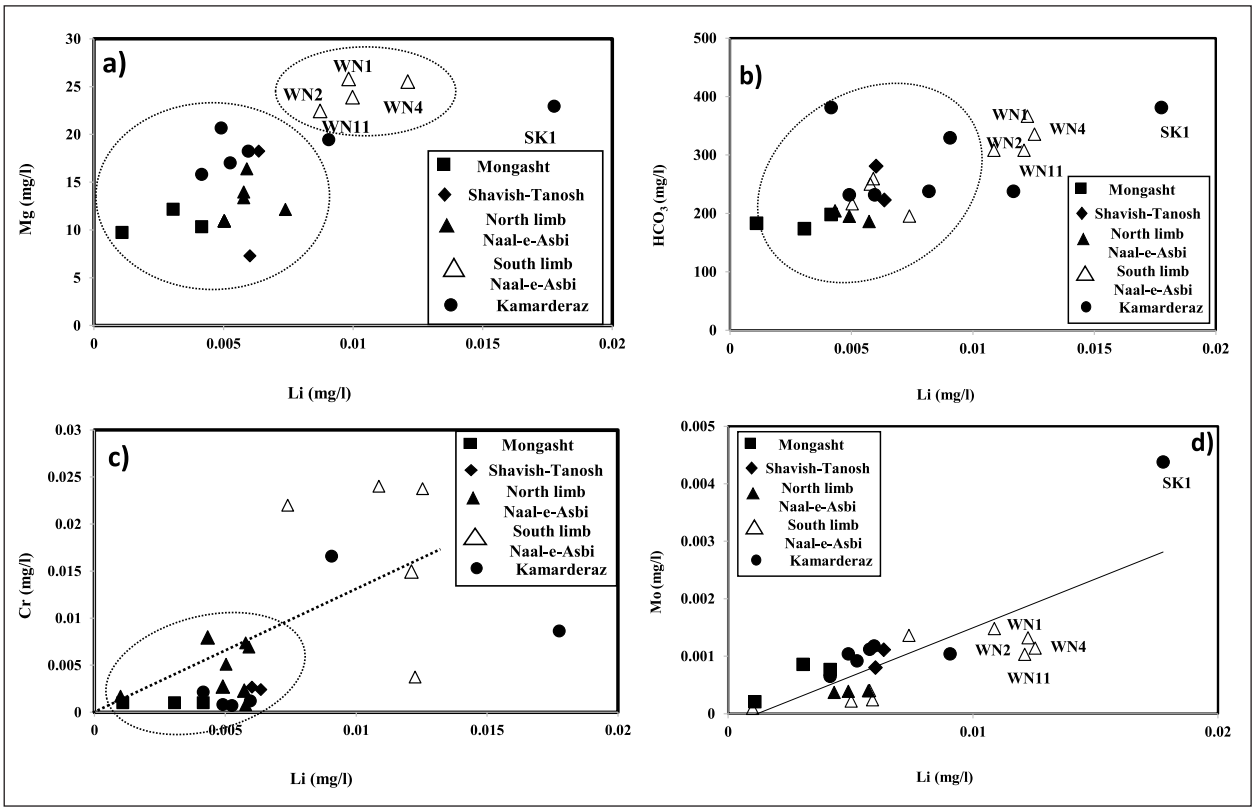

Figure 10: The covariation of Li^{+2} vs. Mg^{+2} (a), HCO_3^- (b), Cr^{+2} (c) and Mo^{+2} (d) in groundwater of the area.

nearby alluvial aquifers, depicting close relationship. The interrelationship of the karstic samples (they are related in terms of hydrochemistry and hydraulic connection) is represented as a cluster or nearly trending pattern, realizing the hydraulic connection among the karstic aquifers. As shown in Figure 10, there is also a good association between the Mongasht samples (SM_1, SM_2, and SM_3) and Shavish-Tanosh (WT_1, WT_2) and the northern part of the Naal-e-Asbi samples (WN). The Southern Naal-e-Asbi and Kamarderaz samples are affected by alluvium recharge water.

3.3. ISOTOPIC CHARACTERISTICS

The oxygen ($\delta^{18}O$) and hydrogen ($\delta^{2}H$), d-excess, temperature and altitude of the sampling points are given in Table 3. The isotopic composition of precipitation ranged between -4.9 to -1.87‰ and -24.14 to -2.9‰ for $\delta^{18}O$ and $\delta^{2}H$ respectively. The local meteoric water line

Table 5: Isotopic values (‰), altitude and temperature of the samples.

NO	Samples	Location	δ^2H (Wet)	$\delta^{18}O$(Wet)	δ^2H (dry)	$\delta^{18}O$(dry)	d-excess	T(°C)	Altitude
1	RA	Mongasht	-9.11	-3.33	-	-	17.53	12.9	1153
2	RAB		-24.14	-4.85	-	-	14.66	12.1	1334
3	RB	Shavish-Tanosh	-4.32	-1.87	-	-	10.64	14.1	681
4	RK_1	Kamarderaz	-8.68	-3.1	-	-	16.12	12.4	889
5	RK_2		-2.9	-2.87	-	-	20.06	13.4	1003
6	RT	Naal-e-Asbi	-18.45	-4.9	-	-	20.75	9.5	973
7	SN_1	Naal-e-Asbi	-12.42	-2.44	-	-	7.1	18	1027
8	WN_1		-15.44	-3.65	-20.14	-5.09	13.76	23	853
9	WN_2		-15.54	-3.5	-19.8	-4.96	12.46	23	847
10	WN_3		-12.29	-3.75	-20.1	-5.03	17.71	22	861
11	WN_4		-14.58	-3.49	-20.77	-5.28	13.34	22	861
12	WN_5		-8.57	-3.62	-21.93	-5.23	20.39	21	859
13	WN_6		-12.65	-3.93	-21.32	-5.06	18.79	22	862
14	WN_7		-14.79	-4.01	-20.66	-4.68	17.29	21.5	839
15	WN_8		-15.13	-4.05	-20.74	-4.42	17.27	22.9	861
16	WN_9		-15.04	-3.84	-20.15	-4.38	15.68	23.7	853
17	WN_{10}		-14.53	-3.8	-16.48	-3.8	15.87	17.8	845
18	WN_{11}		-14.5	-4.05	-18	-3.65	17.9	16.5	920
19	SM_1	Mongasht	-23.04	-5.62	-31.26	-6.32	21.92	12.8	1915
20	SM_2		-21.47	-5.6	-29.33	-5.88	23.33	18	1218
21	SM_3		-27.06	-4.87	-29.47	-5.91	11.9	20	1211
22	WK_1	Kamarderaz	-16.02	-3.98	-23.62	-4.36	15.82	24.6	815
23	WK_2		-19.87	-3.47	-22.22	-3.99	7.89	22.7	819
24	WK_3		-19.37	-3.63	-22.94	-4.11	9.67	24.7	847
25	WK_4		-17.39	-3.58	-22.87	-4.39	11.25	23.2	810
26	SK_1		-22.4	-2.73	-19.79	-3.84	-0.56	24	1037
27	SK_2		-21.97	-2.52	-	-	-1.81	18	1041
28	SK_3		-18.48	-3.07	-21.49	-3.78	6.08	20.9	1121
29	WT_1	Shavish-Tanosh	-18.24	-3.49	-22	-4.56	9.68	23.7	843
30	WT_2		-16.72	-3.61	-22.12	-4.61	12.16	23.7	844
Mean (Groundwater samples)			-16.97	-3.76	-20.3	-4.3	13.12	21.23	958.7

(LMWL) which is placed above the global meteoric water line (GMWL), has a slope less than the GMWL and the position difference is related to local climatic conditions (Figure 11).

Deuterium excess (d-excess) is a second-order stable isotope parameter measured in meteoric water to understand both the source of precipitation and the evolution of moisture during transport. The d-excess precipitation is related to the kinetic fractionation processes that occur during evaporation of water, and is mainly affected by the relative humidity (Jouzel et al., 2007; Bershaw, 2018), temperature in the moisture's source area (Dansgaard et al., 1989; Frohlich & Gibson, 2015), the evaporation conditions (Johnsen et al., 1989; Chen et al., 2004; Masson-Delmotte et al., 2005), and the vapor transport processes. The d-excess therefore can offer insights into the climatic processes at the time the precipitation falls (Dansgaard et al., 1989). Therefore, in general the observed change of deuterium excess is dependent upon humidity, temperature, altitude and evaporation.

The d-excess higher than 20‰ in precipitation sample results from arid vapor sources. The vapor sources of some precipitation samples (RK_2 and RT) are indicating aridity with low humidity. Apart to the low humidity of vapor source the higher d-excess may be due to temperature, altitude difference, evaporation difference and mi-

croclimate conditions. In addition to higher d-excess of precipitation, some groundwater samples, including, well sample (WN_5) and spring samples (SM_1, SM_2 and SM_3) are showing higher d-excess. The reasons for higher d-excess of well and spring sample are well depth and snow melting origin of the springs.

According to the isotopic composition results of the groundwater resources in the area (Table 4), the mean values of $\delta^{18}O$ in wet and dry seasons were -3.76 to -4.3 ‰, and -16.97 to -13.12‰ and the mean $\delta^{2}H$ value in wet and dry seasons were to respectively. The isotopic content of groundwater resources in wet and dry seasons is mostly distributed between the LMWL and GMWL (Figure 11) and based on location; the samples are divided into three groups, with more dispersion on dry season.

The first group is the Mongasht anticline springs, which are placed on the left of the LMWL, depleted and from the rain and snow falling on the heights. These springs have a short residence time due to the conduit nature of the system and rapid movement of groundwater. The second group, including the Shavish-Tanosh and Kamarderaz anticlines and the Naal-e-Asbi samples are positioned parallel to the GMWL and on or below the LMWL. In addition to the rainfall isotopic composition effect, groundwater mixing has also played a role in their isotopic characteristics. In the third group, the samples are situated on the right side of the LMWL or on the GMWL and the most of the water samples belong to the Kamarderaz anticline. Probably, due to the recharge of karst water sources with different systems (conduit and diffuse), longer water retention time in the system and more water-rock interaction, the $\delta^{18}O$ content of these samples have been enriched.

Usually the $\delta^{18}O$ and $\delta^{2}H$ seasonal changes are influenced by the inflow of melted snow in early spring (with a light isotopic index), then relatively richer rainfall in end spring and eventually the evaporation process during summer (Clark & Fritz, 1997; Edwards et al., 2004). It is evident that dry season samples in the area are more depleted than the wet season. This indicates that mostly local rainfall in winter and fracture flow from the Mongasht anticline recharges the karstic aquifers in the lower parts of the area and illustrates the interconnection of the water bearing structures.

The isotopic composition of the groundwater in relation to altitude represents an indicator for locating the groundwater recharge area (Mazor, 2004). The plots of $\delta^{18}O$ and $\delta^{2}H$ values of the samples vs. the corresponding altitude in the area are presented in Figure 15. The altitude effect on isotopic composition of groundwater is expressed by the linear correlation of $\delta^{18}O$ and $\delta^{2}H$ with altitude as given in Equation 1 and 2.

$$\delta^{18}O = -0.001 \text{ Altitude} - 2.338 \qquad \text{[Equation 1]}$$

$$\delta^{2}H = -0.008 \text{ Altitude} - 8.897 \qquad \text{[Equation 2]}$$

The local isotopic gradient shows depletion of stable isotopes by about -0.1‰ and -0.8 ‰ per 100 m elevation for $\delta^{18}O$ and $\delta^{2}H$, respectively (Figure 12). The most depleted samples are in the Mongasht area, while the Naal-e-Asbi and Kamarderaz springs (lowest elevation) are the least depleted ones.

Total dissolved solids (TDS) are a comprehensive image of common ion concentration in groundwater, and also a significant index for dissolution of geological formations, and usually the TDS of groundwater increases in the flow direction. In ideal conditions samples with highest TDS, are generally more enriched in ^{18}O and ^{2}H.

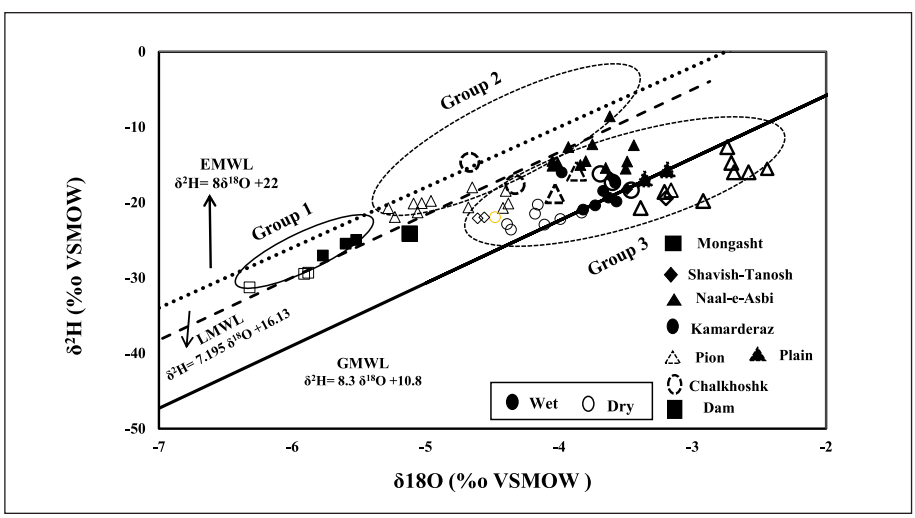

Figure 11: Position of the isotopic composition of groundwater resources in the wet and dry seasons with respect to the local meteoric water line (LMWL) and the global meteoric water line (GMWL).

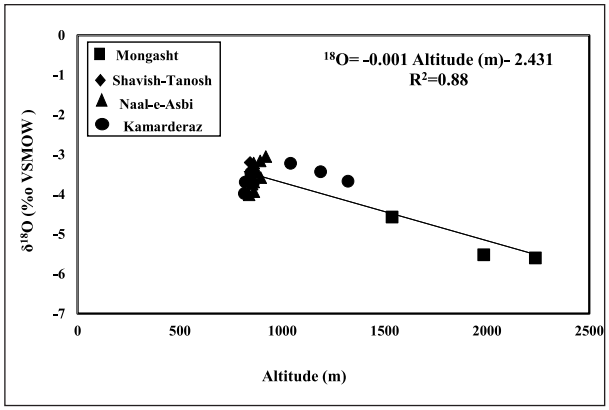

Figure 12: Relationship between $\delta^{18}O$ and elevation of the springs and wells.

Thus, the linear arrays between end-members should be seen on plots of δ^2H and $\delta^{18}O$ vs. TDS (Welhan, 1987). Groundwater is dissolving oxygen-bearing minerals and aggravates the groundwater dissolution formations during the process of flowing (Li et al., 2021). So, the isotope exchange equilibrium equations move leftward (Equation 3) and $\delta^{18}O$ increased in accordance with the increase of TDS value, that is, $\delta^{18}O$ increases in the groundwater flow direction.

$$CaCO_2^{18\,(\text{calcite, dolomite and limestone})} + H_2O \leftrightarrow CaCO_3 + H_2^{18}O \quad \text{[Equation 3]}$$

To represent the ion concentration against isotope ratios, the TDS vs. $\delta^{18}O$ depicted in Figure 13. As shown, the Mongasht samples possess more depleted isotope ratios and lower TDS than the Shavish-Tanosh, Kamarderaz and Naal-e-Asbi samples, and increasing trend of the TDS vs. $\delta^{18}O$ in down gradient which may imply the recharge source of the karstic aquifers from the Mongasht area. In most parts of the catchment diffuse flow occurs and recharge water travels along longer flow paths that lead to increasing residence time, TDS builds up and enhancing water-rock interactions. Thus, discharging water in the lower reaches shows higher ion concentrations and isotope signatures. But in general, during the process of water infiltration, occurrence of isotopes attenuation resulted in to decrease the base flow isotope ratios in dry season.

The content of $\delta^{18}O$ in relation to TDS is more linear than that of δ^2H. Such behavior may suggest water-rock interaction which affects the isotopic composition of pore fluids (Porowski, 2004). The reason for ^{18}O shifting much more than ^2H value is the fact that rock contains a large amount of oxygen, but a very small amount of hydrogen (Bagheri et al., 2021). Of course deviation from a linear relationship (Figure 13) seems to be an evidence of other processes than dissolution which may affect the

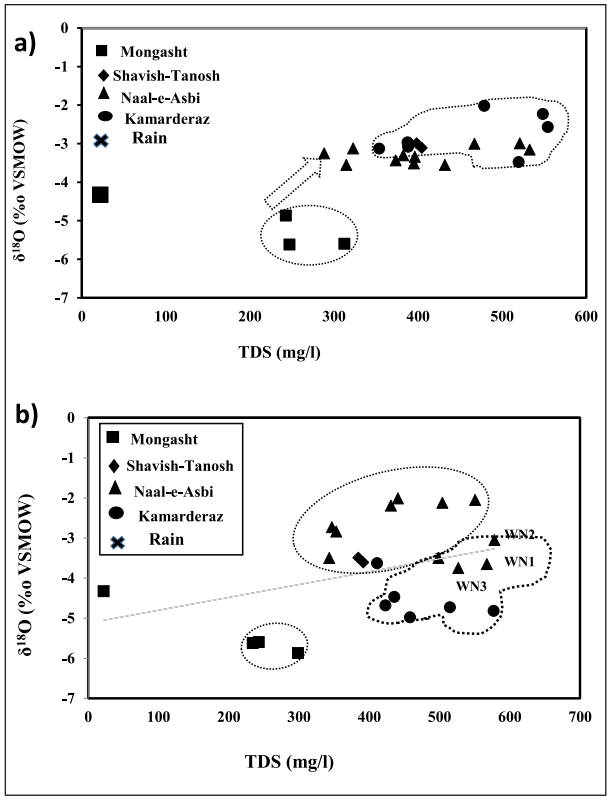

Figure 13: Relationship between $\delta^{18}O$ and TDS (a), and δ^2H and TDS (b), of the springs and wells in the area.

isotopic composition of waters in the carbonate formations such as reversing the flow direction of the nearby alluvial aquifers into karstic horizons and evaporation.

Based on Figure 16 (TDS vs. $\delta^{18}O$ and δ^2H) there is a good relationship between the Mongasht, Naal-e-Asbi and the remaining samples depicting the hydraulic connection and water transport from the Mongasht anticline into the Naal-e-Asbi, Shavish-Tanosh and Kamarderaz aquifers. The water movement from the Mongasht aquifer into the Naal-e-Asbi is clearly observed in the wet season.

The d-excess values of water in the Mongasht anticline are higher than the other waters (Shavish-Tanosh and Kamarderaz anticlines and the Naal-e-Asbi) in the study area (Figure 14). The relatively higher d-excess values of the Mongasht anticline springs (SM_1, SM_2, and SM_3) can be due to the input of snow melt water in addition to precipitation. The reduction of the groundwater d-excess in by increasing the $\delta^{18}O$ values indicates that the groundwater flow in the area is mixed with different degree of infiltrating evaporated water in the flow path. The $\delta^{18}O$ increase with d-excess reduction supports the fact that the evaporation process affecting the isotopic signatures of oxygen and hydrogen.

As shown in Figure 14a-b, ($\delta^{18}O$ vs. d-excess), a close

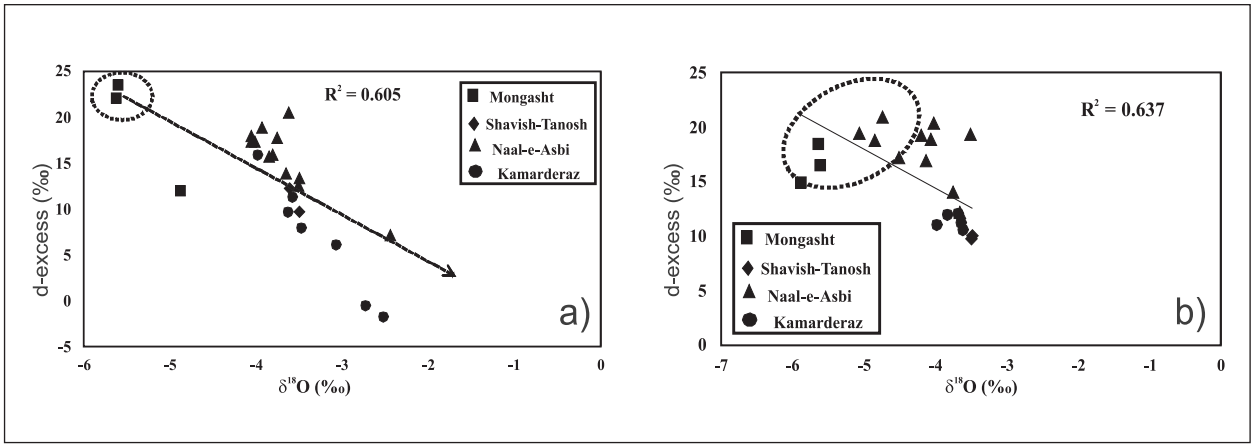

Figure 14: The relationship between d-excess and $\delta^{18}O$ of water samples (wet (a) and dry (b) seasons).

interconnection of the Mongasht anticline with the lower reaches water bearing structures, including Naal-e-Asbi, Shavish-Tanosh and Kamarderaz aquifers is observed. This association supports the role of the Mongasht territory to recharge the nearby aquifers and in particular the Naal-e-Asbi in the wet and dry seasons.

3.4. CONCEPTUAL MODEL OF GROUNDWATER FLOW

From the previous discussion, it is evident that an objective of this study is to develop a framework to identify the hydraulic connection and flow path for groundwater in the area. According to the literature review, the Mesozoic-Cenozoic carbonate complex constitutes the regional karstic aquifer and shails clays represent the regional aquitard. A geological and hydrogeological section between Mongasht anticline has been created to review the hydrogeological conceptual model of the Izeh plain using literature data, new collected data, and the geological reconstruction (Figure 3). Karst wells in Naal-e-Asbi syncline and springs represent the discharge zone of the groundwater flow coming from the movement of water from the higher elevation in the Mongasht territory towards the lower regions, including the Shavish-Tanosh, Kamarderaz and the Naal-e-Asbi aquifers (Figure 15).

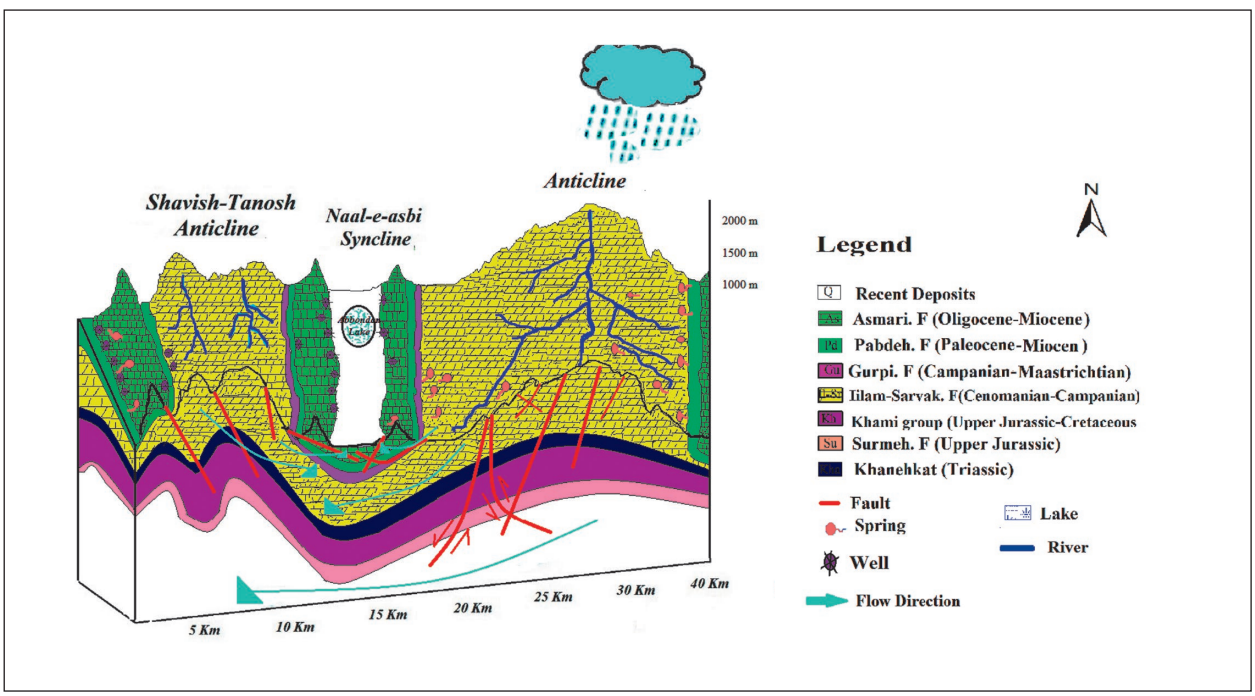

Figure 15: Geological cross section (along A-B located in Figure 1), showing flow path.

4. CONCLUSIONS

Having in mind the fact that Iran is located at the heart of thirst of Middle East, the karst aquifers in the Zagros area are of great economical and social importance and, thus, challenging. The presented dataset is the first compilation of stable isotope hydrological data in Izeh. The water stable isotopes data demonstrate spatial distribution in various hydrogeological settings across the Izeh and provide input for future hydrogeological studies and direction for groundwater management. This research was conducted to assess the hydrochemical characterization and isotopic measurements of the Izeh watershed and also to determine hydraulic relationships among the water bearing structures. The command area recharges mainly from rainfall, but the Mongasht aquifer experiences rejuvenation from rainfall as well as snow. The study results suggest that hydrochemical and isotopic data are applicable to understand the flow paths of springs (e.g., conduit flow through carbonate rocks) and the storage.

The dominant cations and anions in groundwater were Ca^{+2}, Mg^{+2} and HCO_3^-, SO_4^{-2} and the sources of ions are mainly calcite and calcite-dolomite formations. The chemical concentration of ions in the samples of the Shavish-Tanosh and Kamarderaz anticlines and the Naal-e-Asbi syncline were considerably higher than the Mongasht anticline samples. The higher ion concentration, is chiefly on account of the water-rock interaction and relatively longer residence time. The water type is dominantly calcium-bicarbonate, although some samples illustrating Ca-SO_4 facies, display, gaining of carbonate aquifers from the within reach alluvial aquifers. The chemical composition of the principal karst springs and wells are dominantly controlled by precipitation and local rock characteristics including limestone and dolomite embracing groundwater flow. Three interrelated processes controlling water-rock interaction, including; recharge water, dissolution and residence time.

Waters flowing out of specific springs (SK_3, SK_4) and WK_1 (well) located in the Kamarderaz anticline. These waters show a different physico-chemical composition characterized by higher temperatures and electrical conductivity, as well as SO_4^{2-}, Cl^- and Na^+ concentrations. This particular composition probably reflects deeper groundwater flows through the saturated zone of the aquifer and longer residence times in the system, favouring a marked water -rock interaction with mainly evaporitic rocks (sulphates and halite) in the Miosen clayey body (Gachsaran formation). The positive correlation between Mg^{2+} and the ratio SO_4^{2-}/Ca^{2+}in some springs suggests the existence of dedolomitization processes caused by the simultaneous dissolution of gypsum and dolomite. There is a good positive correlation between major and certain trace elements and trace elements itself, displaying hydraulic connection among the karstic aquifers. This hydraulic connectivity is clearly observed between the Mongasht and Shavish-Tanosh anticlines and the Mongasht anticline and the northern limb of the Naal-e Asbi syncline and the Shavish Tanosh anticline and the southern limb of the Naal-e-Asbi syncline.

The Mongasht anticline springs are placed on the higher altitudes with short flow path indicated depleted $\delta^{18}O$ and $\delta^{2}H$ isotopes. While the Kamarderaz and Shavish-Tanosh anticlines and the Naal-e-Asbi samples, as a result of merely rainfall recharge, diffuse flow, longer travel path, more water-rock interaction and groundwater mixing are showing relative isotopic enrichment.

The combination of this gradient with the mean $\delta^{18}O$ signature of the water drained by the springs has allowed an estimate of the average recharge altitude for each spring and karstic wells.

The results are congruent with the topographic distribution of permeable areas and the position of the springs and karstic wells. In addition, they allow assumptions regarding the flow paths of groundwater drained by different springs and a possible hydrogeological connection of the Izeh aquifers with the adjacent permeable outcrops. The TDS vs. $\delta^{18}O$ indicate that the most depleted isotopic values and the lowest ion concentration are in the Mongasht samples as compare to the Kamarderaz, Shavish-Tanosh and the Naal-e-Asbi samples, illustrating the importance of the Mongasht anticline to recharge the lower reaches of the area.

The d-excess value of the Mongasht anticline samples is higher than the other samples, including the Kamarderaz and Shavish-Tanosh anticline and the Naal-e-Asbi syncline. The decreasing amount of groundwater d-excess by increasing of $\delta^{18}O$ signature shows that the groundwater is mixed with different degrees of percolated evaporated recharge water in the flow direction from the Mongasht anticline to the lower reaches.

The collected results from the major ions, trace elements, correlation coefficients, composite diagrams, $\delta^{18}O$, $\delta^{2}H$ and d-excess values along with a hydrogeological cross section reveal common origin of water, flow pattern and interconnection among the geological structures.

ACKNOWLEDGMENTS

The authors are so much grateful to the vice chancellor for the research of Shahid Chamran University of Ahvaz for providing financial assistance (grant no SCU. EG 99.618) and also would like to thank the exploitation deputy of Khuzestan Water and Power Authority (KWPA) for financial support and imparting necessary data to conduct this research.

5. REFERENCES

Alavi, N.M., 1996. Tectonic of the Zagros, organic belt of Iran, new data and interpretation. Tectonophysics, 299: 211–238.

Alemayehu, T., Leis, A., Dietzel, M., 2020. Environmental isotope and hydrochemical characteristics of groundwater in central portion of Mekelle sedimentary outlier, northern Ethiopia. Journal of African Earth Sciences, 171: 103953. https://doi.org/10.1016/j.jafrearsci.2020.103953.

Alfarrah, N., Walraevens, K., 2018. Groundwater overexploitation and seawater intrusion in coastal areas of arid and semi-arid regions. Water, 10(2): 143. https://doi.org/10.3390/w10020143.

Ashjari, J., Raeisi, E., 2006. Anticline structure influences on regional flow, Zagros, Iran. Journal of cave and karst studies, 68(3): 118-129.

Badaruddin, S., Werner, A.D., Morgan, L.K., 2017. Characteristics of active seawater intrusion Journal of Hydrology, 551: 632-647. https://doi.org/10.1016/j.jhydrol.2017.04.031.

Bagheri, F., Karami, G.H., Bagheri, R., Griffioen, J., Eggenkamp, H., Jafari, H., 2021. Geochemical and multi-isotopes ($\delta^{18}O$, $\delta^{2}H$, $\delta^{13}C$, 3H and $\delta^{37}Cl$) evidences to karst development and flow directions in Tran's boundary aquifer, Northeast of Iran. Applied Geochemistry, 132: 105071. https://doi.org/10.1016/j.apgeochem.2021.105071.

Bajjali, W., 2006. Recharge mechanism and hydrochemistry evaluation of groundwater in the Nuaimeh area, Jordan, using environmental isotope techniques. Hydrogeology Journal, 14(1): 180-191. http://dx.doi.org/10.1007/s10040-004-0352-2.

Bershaw, J., 2018. Controls on Deuterium Excess across Asia. Geosciences, 8(7): 257. https://doi.org/10.3390/geosciences8070257.

Bhat, N.A., Jeelani, G.H., 2015. Delineation of the recharge areas and distinguishing the sources of karst springs in Bringi watershed, Kashmir Himalayas using hydrochemistry and environmental isotopes. Journal of Earth System Science, 124: 1667–1676. https://doi.org/10.1007/s12040-015-0629-y.

Blasch, K.W., Bryson, J.R., 2007. Distinguishing sources of ground water recharge by using delta ^{2}H and delta^{18}O. Ground Water, 45(3): 294– 308. https://doi.org/10.1111/j.1745-6584.2006.00289.x.

Bourke, S., Hammond, M., Clohessy, S., 2015. Perth shallow groundwater systems investigation: North Lake. http://www. water.wa.gov.au/Publication Store/first/91255.pdf [Accessed May 2015].

Celle-Jeanton, H., Travy, Y., Blavoux, B., 2001. Isotopic typology of the precipitation in the Western Mediterranean region at three different time scales. Geophysical Research Letters, 28: 1215–1218.

Chen, J., S, Li, L., Wang, J.Y., Barry, D.A., Sheng, X.F., Gu, W.Z., Zhao, X., Chen, L., 2004. Water resources: groundwater maintains dune landscape. Nature, 432: 459–460. https://doi.org/10.1038/432459a

Chen, W., Li, H., Hou, E., Wang, S., Wang, G., Panahi, M., Li, T., Peng, T., Guo, C., Niu, C., 2018. Gis-based groundwater potential analysis using novel ensemble weights-of-evidence with logistic regression and functional tree models. Science of Total Environment, 634: 853–867. https://doi.org/10.1016/j.scitotenv.2018.04.055.

Chihi, H., Marsily, G., Belayouni, H., Yahyaoui, H., 2015. Relationship between tectonic structures and hydrogeochemical compartmentalization in aquifers: example of the Jeffara de Medenine system, south-east Tunisia. Journal of Hydrology: Regional Studies, 4: 410–430. https://doi.org/10.1016/j.ejrh.2015.07.004.

Ciner, F., Sunkari, E.D., Senbas, B.A., 2021. Geochemical and Multivariate Statistical Evaluation of Trace Elements in Groundwater of Nigde Municipality, South-Central Turkey: Implications for Arsenic Contamination and Human Health Risks Assessment. Archives of Environmental Contamination and Toxicology, 80: 164–182. https://doi.org/10.1007/s00244-020-00759-2.

Clark, I.D., Fritz, P., 1997. Environmental Isotopes in Hydrogeology. 1st Edition. CRC Press, USA, 352 pp.

Connor J.A., Paquette, S., Mchugh, T., Gie, E., Hemingway, M., Bianchi, G., 2017. Application of natural resource valuation concepts for development of sus-

tainable remediation plans for groundwater. Journal of Environmental Management, 204: 721. https://doi.org/10.1016/j.jenvman.2017.03.053.

Coplen, T. B., 1993, 'Uses of Environmental Isotopes', in: Alley, W. M. (ed.), Regional Water Quality, Van Nostrand Reinhold, pp. 227–254.

Dansgaard, W., White, J.W., Johnsen, S.J., 1989. The abrupt termination of the Younger Dryas climate event. Nature, 339: 532–534.

Dimitriou, E., Tsintza, P., 2015. Hydrogeologic Investigations in Western Crete by Using Isotopic Analyses and GIS Techniques. Journal of Water Resource and Protection, 7: 923-937. http://dx.doi.org/10.4236/jwarp.2015.712076.

Doctor, D.H. Jr, Alexander, C.E. Jr, Petric, M., Kogovsek, J., 2006. Quantification of karst aquifer discharge components during storm events through end-member mixing analysis using natural chemistry and stable isotopes as tracers. Hydrogeology Journal, 14(7): 1171-1191. https://doi.org/10.1007/s10040-006-0031-6.

Doveri, M., Menichini, M., Cerrina Feroni, A., 2013. Stable water isotopes as fundamental tool in karst aquifer studies: some results from isotopic applications in the Apuan Alps carbonatic complexes (NW Tuscany). Italian Journal of Engineering Geology and Environment, 1: 33–50. http://dx.doi.org/10.4408/IJEGE.2013-01.O-03.

Edmunds, W.M., Ma, J.Z., Aeschbach-Hertig, W., Kipfer, R., Darbyshire, D.P.F., 2006. Groundwater recharge history and hydrogeochemical evolution in the Minqin Basin, North West China. Applied Geochemistry, 21(12): 2148–2170.

Edwards, T.W.D., Wolfe, B.B., Gibson, J.J., Hammarlund, D., 2004. Use of water isotope tracers in high-latitude hydrology and paleohydrology. In: Pienitz, R., Douglas, M.S.V., Smol, J.P. (Eds.), Long-term Environmental Change in Arctic and Antarctic Lakes. Springer, Dordretch, pp. 187–207.

Emblanch, C., Zuppi, G.M., Mudry, J., Blavoux, B., Batiot, C., 2003. Carbon 13 of TDIC to quantify the role of the unsaturated zone: the example of the Vaucluse karst systems (Southeastern France). Journal of Hydrology, 279(1-4): 262–274. http://dx.doi.org/10.1016/S0022-1694 (03)00180-X.

Fairchild, I.J., Borsato, A., Tooth, A.F., Frisia, S., Hawkesworth, C.J., Huang, Y, McDermott F.P., Spiro, B., 2000. Controls on trace element (Sr–Mg) compositions of carbonate cave waters: implications for speleothem climatic records. Chemical Geology, 166: 255–269.

Farid, I., Abbas, M.H.H., Bassouny, M., 2020. Indirect impacts of irrigation with low quality water on the environmental safety. Egyptian Journal of Soil Science, 60(1):1-15. https:// doi. Org/ 10. 21608/ ejss. 2019. 15434. 1294.

Ford, D.C., Williams, P.W., 1989. Karst Geomorphology and Hydrology. Unwin Hyman, London: Chapman and Hall, 601 pp.

Ford, D.C., Williams, P.W., 2007. Karst Hydrogeology and Geomorphology. John Wiley, Chichester, 562 pp. https://doi.org/10.1002/9781118684986

Frohlich, K., Gibson, J.J., 2015. Aggarwal, P. Deuterium Excess in Precipitation and Its Climatological

Significance. Available online: http://www.iaea.org/inis/collection/NCLCollectionStore/_Public/

34/017/34017972.pdf (Accessed 12 March 2015).

Gates, J.B., Edmunds, W.M., Darling, W.G., Pang, J., Ma, Z., Young, A.A., 2008. Conceptual model of recharge to southeastern Badain Jaran Desert groundwater and lakes from environmental tracers. Applied Geochemistry, 23(12): 3519– 3534. http://dx.doi.org/10.1016/j.apgeochem.2008.07.019.

Gibbs, R.J., 1970. Mechanisms controlling world water chemistry. Science, 17: 1088–1090.

Goldscheider, N., Andreo, B., 2007. The geological and geomorphological framework. In: Goldscheider, N., Drew, D. (Eds.), Methods in karst hydrogeology. International Contribution to Hydrogeology, IAH, vol 26. Taylor and Francis/Balkema, London, pp. 9–23.

Haldar, K., Kujawa-Roeleveld, K., Dey, P., 2020. Spatio-temporal variations in chemical-physical water quality parameters influencing water reuse for irrigated agriculture in tropical urbanized deltas. Science of the Total Environment, 708: 134559. https:// doi.o rg/1 0.1 016/j. scito tenv. 2019. 134559.

Hatipoglu-Bagci, Z., Sazan, M.S., 2014. Characteristics of karst springs in Aydıncık (Mersin, Turkey), based on recession curves and hydrochemical and isotopic parameters. Quarterly Journal of Engineering Geology and Hydrogeology, 47(1): 89-99. https://doi.org/10.1144/qjegh2013-074.

Helena, B., Pardo, R., Vega, M., Barrado, E., Fernandez, J.M., Fernandez, L., 2000. Temporal evolution of groundwater composition in an alluvial (Pisuerga river, Spain) by principal component analysis. Water Research, 34: 807–816.

Heydarizad, M., Minaei, F., Eskandari Mayvan, J., Mofidi, A., Minaei, M., 2021. Spatial distribution of stable isotopes (18O and 2H) in precipitation and groundwater in Iran, Isotopes in Environmental and Health Studies, 57(4): 400-419. https://doi.org/10.1080/10256016.2021.1924167.

Hounslow, A.W., 1995. Water Quality Data: Analysis and Interpretation, CRC Lewis Publishers, Boca Raton, pp. 86–87.

Jebreen, H., Banning, A., Wohnlich, S., Niedermayr, A., Ghanem, M., Wisotzky, F., 2018. The Influence of Karst Aquifer Mineralogy and Geochemistry on Groundwater Characteristics: West Bank, Palestine. Jornal Water, 10: 1829. https://doi.org/10.3390/w10121829.

Jiang, L., Sui, M., Fan, Y., Su, H., Xue, Y., Zhong, S., 2021. Micro-gas column assisted laser induced breakdown spectroscopy (MGC-LIBS): A metal elements detection method for bulk water in-situ analysis. Spectrochimica Acta Part B: Atomic Spectroscopy, 177: 106065. https://doi.org/10.1016/j.sab.2021.106065.

Johnsen, S.J., Dansgaard, W., White, J.W.C., 1989. The origin of Arctic precipitation under present and glacial conditions. Tellus B, 41: 452–468.

Jouzel, J., Stievenard, M., Johnsen, S.J., Landais, A., Masson-Delmotte, V., Sveinbjornsdottir, A., Vimeux, F., von Grafenstein, U., White J.W.C., 2007. The GRIP deuteriumexcess record. Quaternary Science Reviews 26(1–2): 1–17. https://doi.org/10.1016/j.quascirev.2006.07.015.

Kalantari, N., Pawar, N.J., Keshavarzi, M.R., 2009. Water resource management in the intermountain Izeh Plain, Southwest of Iran. Journal of Mountain Science, 6: 25–41. https://doi.org/10.1007/s11629-009-0212-6.

Krienen, L., Heuser, M., Hobig, N., 2017. Hydrogeological and hydrochemical characterization of two karstic discharge areas in San Luis Potosí, Mexico. Environmental Earth Sciences, 76: 825. https://doi.org/10.1007/s12665-017-7166-8.

Langelier, W.F., Ludwig, H.F., 1942. Graphic method for indicating the mineral character of natural water.

Journal - American Water Works Association, 34(3): 335–352.

Lewinska-Preis, L., Szram, E., Fabiańska, M.J., 2021. Selected ions and major and trace elements as contaminants in coal-waste dump water from the Lower and Upper Silesian Coal Basins (Poland). International Journal of Coal Science & Technology, 8: 790–814. https://doi.org/10.1007/s40789-021-00421-9.

Li, X., Han, G., Liu, M., Liu, J., Zhang, Q., Qu, R., 2021. Potassium and its isotope behaviour during chemical weathering in a tropical catchment affected by evaporite dissolution, Geochimica et Cosmochimica Acta, 316: 105-121. https://doi.org/10.1016/j.gca.2021.10.009.

Liu, P., Yang, M., Sun, Y., 2019. Hydro-geochemical processes of the deep Ordovician groundwater in a coal mining area, Xuzhou, China. Hydrogeology, 27(6): 2231-2244. https://doi.org/ 10.1007/s10040-019-01991-4.

Ma, J.Z., He, J.H., Qi, S., Zhu, G.F., Zhao, W., Edmunds, W.M., Zhaom, Y.P., 2013. Groundwater recharge and evolution in the Dunhuang Basin, northwestern China. Applied Geochemistry, 28:19–31.

Mahlknecht, J., Garfias-Solis, J., Aravena, R., Tesch, R., 2006. Geochemical and isotopic investigations on groundwater residence time and flow in the Independence Basin, Mexico. Journal of Hydrology, 324(1-4): 283–300. http://dx.doi.org/10.1016/j.jhydrol.2005.09.021.

Makhloufi, Y., Rusillon, E., Brentini, M., Moscariello, A., Meyer, M., Samankassou, E., 2018. Dolomitization of the Upper Jurassic carbonate rocks in the Geneva Basin, Switzerland and France. Swiss Journal of Geosciences, 111: 475–500. https://doi.org/10.1007/s00015-018-0311-x.

Marfia, A.M., Krishnamurthy, R.V., Atekwana, E.A., Panton, W.F., 2004. Isotopic and geochemical evolution of groundwater and surface waters in a karst-dominated geological setting: a case study from Belize, Central America. Applied Geochemistry, 19: 937–946. https://doi.org/10.1016/j.apgeochem.2003.10.013.

Masson-Delmotte, V., Jouzel, J., Landais, A., Stievenard, M., Johnsen, S.J., White, J.W.C., Werner, M., Sveinbjornsdottir, A., Fuhrer, K., 2005. GRIP deuterium excess reveals rapid and orbital-scale changes in Greenland moisture origin. Science, 309(1): 118–121.

Mazor, E., 2004. Chemical and isotopic groundwater hydrology, 3rd ed. Weizmann Institute of Science Rehovot, New York, 465pp.

Milanovic, P.T., 1981. Karst hydrogeology. Water Resources publications, Littleton, 434 pp.

Mokadem, N., Dennis, R., Dennis, I., 2021. Hydrochemical and stable isotope data of water in karst aquifers during normal flow in South Africa. Environmental Earth Sciences, 80: 519. https://doi.org/10.1007/s12665-021-09845-7.

Moral, F., Cruz-Sanjulian, J.J., Olias, M., 2008. Geochemical evolution of groundwater in the carbonate aquifers of Sierra de Segura (Betic Cordillera, southern Spain). Journal of Hydrology, 360: 281– 296.

Morsy, K.M., Morsy, A.M., Hassan, A.E., 2018. Groundwater sustainability: opportunity out of threat. Groundwater for sustainable development, 7: 277–285.

Murillo, R.S., Brooks, E., Elliot, J.W., Bolla, J., 2015. Isotope hydrology and baseflow geochemistry in natural and human-altered watersheds in the inland Pacific Northwest, USA. Isotopes in Environmental and Health Studies, 51(2): 231–254. https://doi.org/10.1080/10256016.2015.1008468.

Nader, F.H., Swennen, R., Ottenburgs, R., 2003. Karst-

meteoric dedolomitization in Jurassic carbonates, Lebanon. Geologica Belgica, 6: 3–23.

Narany, S.T., Ramli, M.F., Aris, A.Z., Sulaiman, W.N.A., Juahir, H., Fakharian, K., 2014. Identification of the hydrogeochemical processes in groundwater using classic integrated geochemical methods and geostatistical techniques in Amol-Babol plain, Iran. Scientific World Journal, 2014: 1–15. https://doi.org/10.1155/2014/419058.

Nassery, H.R., Alijani, F., Nakhaei, M., 2013. The comparison of hydrodynamic characteristics of karst aquifers: application on two karst formations in Zagros (Asmari and Ilam-Sarvak), southwest Iran. Arabian Journal of Geosciences, 7(11): 4809-4818. http://dx.doi.org/10.1007%2Fs12517-013-1017-z.

Negrel, Ph, Petelet-Giraud, E., 2005. Strontium isotopes as tracers of groundwater induced floods: the Somme case study (France). Journal of Hydrology, 305: 99. 119. https://doi.org/10.1016/j.jhydrol.2004.08.031.

Porowski, A., 2004. Isotopic evidence of the origin of mineralized waters from the Central Carpathian Synclinorium, SE Poland. Environmental Earth Sciences, 46(5): 661-669.http://dx.doi.org/10.1007/s00254-004-1005-4.

Pracny, P., Faimon, J., Vsiansky, D., 2017. Evolution of Mg/Ca Ratios during Limestone Dissolution under Epikarstic Conditions. Aquatic Geochemistry, 23: 119–139. https://doi.org/10.1007/s10498-017-9313-y.

Pratama, A.D., Dwiputra, D.S., Nurkholis, A., Haryono, E., Cahyadi, A., Fauzan, R., 2021. Factors Affecting Hydrochemistry of Karst Springs and their Relationship to Aquifer Development. Environmental Processes, 8: 1379–1413. https://doi.org/10.1007/s40710-021-00547-7.

Rademacher, L.K., Clark, J.F., Boles, J.R., 2003. Groundwater residence times and flow paths in fractured rock determined using environmental tracers in the Mission tunnel: Santa Barbara County, California, USA. Environ Geol 43: 557–567.

Rajmohan, N, Elango, L., 2004. Identification and evolution of hydrogeochemical processes in the groundwater environment in an area of the Palar and Cheyyar river basins, southern India. Environmental Geology, 46(1): 47–61. https://doi.org/10.1007/s00254-004-1012-5.

Rehman, F., Cheema, T., Azeem, T., 2019. Groundwater quality of Sargodha city and its suitability for domestic and irrigation purpose. Fresenius Environmental Bulletin, 28(11): 7695–7700.

Ren, M., Jones, B., 2017. Spatial variations in the stoichiometry and geochemistry of Miocene dolomite from Grand Cay-man: implications for the origin of island dolostone. Sedimentary Geology, 348: 69–93. https://doi.org/10.1016/j.sedgeo.2016.12.001.

Rodgers, P., Soulsby, C., Waldron, S., Tetzlaff, D., 2005. Using stable isotope tracers to assess hydrological flow paths, residence times and landscape influences in a nested mesoscale catchment. Hydrology and Earth System Sciences, 9: 139–155. https://doi.org/10.5194/hess-9-139-2005.

Rudy, L., Maheu, C., Korner, A., Lebel, S., Gelinas, C., 2020. The FCR-1: Initial validation of a single-item measure of fear of cancer recurrence. Psychooncology, 29(4): 788-795. https://doi.org/10.1002/pon.5350.

Ryu, J.S., Lee, K.S., Chang, H.W, 2007. Hydrogeochemical and isotopic investigations of the Han River basin, South Korea. Journal of Hydrology, 345(1-2): 50–60. https://doi.org/10.1016/j.jhydrol.2007.08.001

Scanlon, R., Healy, W., Cook, G., 2002. Choosing appropriate techniques for quantifying groundwater recharge. Hydrogeology. Journal, 10(1): 18–39. http://dx.doi.org/10.1007/s10040-001-0176-2.

Setiawan, T., Yoseph, C.S.S.B., Alam, S., Haryono, E., Hendarmawan, I., 2020. Hydrochemical and environmental isotopes analysis for characterizing a complex karst hydrogeological system of Watuputih area, Rembang, Central Java, Indonesia, Hydrogeology Journal, 28(5): 1635-1659. https://ui.adsabs.harvard.edu/link_gateway/2020HydJ...28.1635S/doi:10.1007/s10040-020-02128-8.

Singh, M., Kumar, S., Kumar, B., Singh, S., Singh, I.B., 2013. Investigation on the hydrodynamics of Ganga alluvial plain using environmental isotopes: a case study of the Gomati River basin, northern India. Hydrogeology Journal, 21: 687–700. https://doi.org/10.1007/s10040-013-0958-3.

Slabe, T., Liu, H., 2009. Significant subsoil rock forms. In: Ginés, A., Knez, M., Slabe, T., Dreybrodt, W., (Eds), Karst rock features, Karren sculpturing. Carsologica, 9. ZRC Publishing, Ljubljana, pp 123–137.

Srivastava, S.K., Ramanathan, A.L., 2008. Geochemical assessment of groundwater quality in vicinity of Bhalswa landfill, Delhi, India, using graphical and multivariate statistical methods. Environmental Geology, 53: 1509–1528.

Stocklin, J., 1974. Evolution of the continental margins bounding a former Southern Tethys. In:Burk, C.A., Drake, C.L.(Eds.), The Geology of Continental Margins. Berlin, Springer, pp. 873-887.

Sun, Z., Ma, R., Wang, Y., Ma, T., Liu, Y., 2016. Using isotopic, hydrogeochemical-tracer and temperature data to characterize recharge and flow paths in a complex karst groundwater flow system in north-

ern China. Hydrogeology Journal, 24: 1393–1412. https://doi.org/10.1007/s10040-016-1390-2.

Tang, L., Zhao, Y., Zhang, S., Sun, T., KaiHu, L., Ming, X., Sheng, Y., Zeng, T., 2021. Origin and evolution of a porphyry-breccia system: Evidence from zircon U-Pb, molybdenite Re-Os geochronology, in situ sulfur isotope and trace elements of the Qiyugou deposit, China. Gondwana Research, 89: 88-104.

Tian, L., Gao, Y., Yang, G., Schwartz, B., Cai, B., Lei, G., Shi, G., Ray, C., Sok, S., Martinez, E., Li, Y., Wu, H., 2021. The evolution of hydrochemical and isotopic signatures from precipitation, surface water to groundwater in a typical karst watershed, Central Texas, USA, Isotopes in Environmental and Health Studies, 57(5): 492-515. https://doi.org/10.1080/10256016.2021.1948410.

Tillman, F.D., Oki, D.S., Johnson, A.G., Barberm, L.B., Beisner, K.R., 2014. Investigation of geochemical indicators to evaluate the connection between inland and coastal groundwater systems near Kaloko-Honoko-hau National Historical Park, Hawai'i. Applied Geochemistry, 51: 278–292. https://doi.org/10.1016/j.apgeochem.2014.10.003.

Valdes, D., Dupont, J.P., Laignel, B., Ogier, S., Leboulanger, T., Mahler, B.J., 2007. A spatial analysis of structural controls on karst groundwater geochemistry at a regional scale. Journal of Hydrology, 340: 244–255. https://doi.org/10.1016/j.jhydrol.2007.04.014.

Ventura-Houle, R., Guevara-Mansilla, O., Requena-Lara, G., 2021. Hydrochemistry, δD and $\delta^{18}O$ to explain the distribution of water quality in a karst setting in the semi-arid region of Northeast Mexico. Environmental Earth Sciences, 80(1): 6. https://doi.org/10.1007/s12665-020-09310.

Vreca, P., Kern, Z., 2021. Use of Water Isotopes in Hydrological Processes. Water, 12(8): 2227.

Wang, Y., Song, X., Li, B., 2018. Temporal variation in groundwater hydrochemistry driven by natural and anthropogenic processes at a reclaimed water irrigation region. Hydrology Research, 49(5):1652–1668. https://doi.org/10.2166/nh.2018.123.

Welhan, J.A., 1987. Stable isotope hydrology. In: Kyser, T.K., (Ed.), Stable Isotope Geochemistry of Low Temperature Processes. Short Course Handbook, 13. Mineralogical Association of Canada, Saskatoon, pp. 129–157.

White, W.B., 2015. Chemistry and karst. Acta Carsologica, 44(3): 349–362. https://doi.org/10.3986/ac.v44i3.1896.

Yasin, D., Kargın, M., 2021. Hydrogeochemical and isotopic characteristics of water resources in Cubuk-Meliksah (Ankara/Turkey). Environmental Earth Science, 80: 513 https://doi.org/10.1007/s12665-021-09813-1.

Yuan, R., Wang, S., Wang, V., Song, X., Tang, C., 2017. Changes in flow and chemistry of groundwater heavily affected by human impacts in the Baiyangdian catchment of the North China Plain. Environmental Earth Sciences, 76(16): 571. https://link.springer.com/article/10.1007%2Fs12665-017-6918-9.

Zaidi, F.K., Nazzal, Y., Jafri, M.K., Naeem, M., Ahmed, I., 2015. Reverse ion exchange as a major process controlling the groundwater chemistry in an arid environment: a case study from northwestern Saudi Arabia. Environmental Monitoring and Assessment, 187(10): 607. https://doi.org/10. 1007/s10661-015-4828-4.

Zanchi, A., Zanchetta, S., Berr, F., Mattei, M., Garzanti, E., Molyneux, S., Sabouri, J., 2009. The Eo-Cimmerian (Late? Triassic) orogeny in North Iran. In: Brunet, M.F.; Wilmsen, F.; Granath, J.W., (Eds.), South Caspian to Central Iran basins. Geological Society Special Publications, 312. Geological Society of London, London, pp. 31-55. https://doi.1.org/10.1144/SP312.3.

Zhang, W., Li, L., Wang, X., Xing, W., Li, R., Yang, T., Lv, D., 2020. Role of trace elements in anaerobic digestion of food waste: Process stability, recovery from volatile fatty acid inhibition and microbial community dynamics. Bioresource Technology, 315: 123796. https://doi.org/10.1016/j.biortech.2020.123796.

Zhou, J., Zhang, Y., Zhou, A., Liu, C., Cai, H., Liu, Y., 2016. Application of hydrochemistry and stable isotopes ($\delta^{34}S$, $\delta^{18}O$ and $\delta^{37}Cl$) to trace natural and anthropogenic influences on the quality of groundwater in the piedmont region, Shijiazhuang, China. Applied Geochemistry, 71: 63–72. https://doi.org/10.1016/j.apgeochem. 2016.05.018.

CONFLICT OF INTEREST

The authors have no conflicts of interest to declare. All co-authors have seen and agree with the contents of the manuscript and there is no financial interest to report. We certify that the submission is original work and is not under review at any other publication. Author names: Nasrollah Kalantari, Zahra Sajadii, Abbas Charchi and Seyyed Sajedin Mousavi.